International Journal of Biological Macromolecules 283 (2024) 137921

Contents lists available at ScienceDirect

International Journal of Biological Macromolecules

journal homepage: www.elsevier.com/locate/ijbiomac

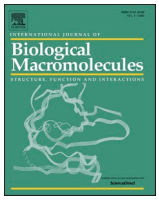

Design and synthesis of a new recyclable nanohydrogel based on chitosan for Deltamethrin removal from aqueous solutions: Optimization and modeling by RSM-ANN

Hossien Rasouli [a], Negin Sohrabi [a,b], Reza Mohammadi [a,*]

[a] Polymer Research Laboratory, Department of Organic and Biochemistry, Faculty of Chemistry, University of Tabriz, Tabriz, Iran
[b] Department of Biosystem Engineering, Faculty of Agriculture, University of Tabriz, Tabriz, Iran

ARTICLE INFO

Keywords:
Chitosan
Deltamethrin
Response Surface Methodology
Hydrogel
Artificial neural network

ABSTRACT

In this study, a new magnetic biocompatible hydrogel was synthesized as an adsorbent for Deltamethrin pesticide removal. The optimal conditions and adsorption process of Deltamethrin by chitosan/polyacrylic acid/Fe_3O_4 nanocomposite hydrogel was studied by Response Surface Methodology by Central Composite Design (RSM-CCD) and Artificial Neural Network (ANN). This adsorbents were synthesized, and then characterized and investigated using FT-IR, XRD, FE-SEM, EDX, Map, VSM, and TGA methods. The results of these analyses showed that the nanocomposite hydrogel was well synthesized and has the ability to adsorb the Deltamethrin pesticide. The results obtained through analysis using response surface methodology showed that the maximum amount of adsorption was 99.79 % at 26 °C, while pH, initial concentration, contact time, and adsorbent dose were 7, 22 ppm, 90 min, and 1.3 g/L respectively. Comparison between results obtained from CCD modeling and artificial neural network proved that both methods had high ability to predict the adsorption process but the CCD method had higher coefficient of determination and lower error. The equilibrium and kinetic study of the process showed that the Toth isotherm model, pseudo-second-order is all suitable for expressing the adsorption process. In addition, the adsorption mechanism followed double-exponential model that combines external and internal diffusions. Results of Thermodynamic study suggested that the Deltamethrin adsorption on CS/PAA/Fe_3O_4 was a spontaneous and exothermic process. The results of the equilibrium process study revealed that the adsorption process was physical and desirable, therefore, the adsorption-desorption process was performed which showed that the composite was reusable up to 10 cycles.

1. Introduction

Polymers are made up of a large number of monomers. Today, it is difficult to imagine an advanced world without polymeric materials, because these materials have become part of our lives, and in the construction of various objects, complex medical, scientific, and industrial tools are used [1]. Polymers are divided into three groups in terms of source, which are natural, semi-synthetic, and synthetic polymers. Natural polymers are obtained from nature and include plant and animal sources [2,3]. Natural polymers such as cellulose families, proteins, polysilicates, nucleic acids, and polysaccharides are divided [4]. Chitosan is a natural polysaccharide with structural properties similar to glycose aminoglycans, non-toxic and biodegradable [5]. Hydrogels are composed of cross-linked and hydrophilic polymer networks [6]. In addition, hydrogels based on natural polymers are reinforced with nanoparticles Therefore; their tension to tensile and compressive stresses is higher than other hydrogels [7,8]. Polymer nanocomposite hydrogels is a group of hydrogels has a composite structure and hydrogels together and have mechanical, physical, chemical, electrical, thermal, and biological properties that are very suitable [9]. Because acrylic acid has a negative charge and chitosan has a positive charge with amine groups, it is thought that a proper interaction occurs between them [10]. Moreover, magnetic nanocomposites based on natural polymer materials are used due to their accessibility, low expense, and high capability to adsorb pesticides [11]. Pesticides have a detrimental effect on humans and the environment [12,13] and are known as the most common and dangerous water pollution [14,15]. Pyrethroid insecticides are one of the most common pesticides effective in the

* Corresponding author.
E-mail address: r.mohammadi@tabrizu.ac.ir (R. Mohammadi).

https://doi.org/10.1016/j.ijbiomac.2024.137921
Received 30 June 2023; Received in revised form 23 September 2023; Accepted 19 November 2024
Available online 21 November 2024

pesticide industry [16,17]. Deltamethrin is one of the most potent and widely used types of Pyrethroid insecticides and are used to control and protect a wide range of crops, fruits, vegetables and aquatic animals against pests and parasites [18,19]. Due to the presence of the CN group in the structure of Deltamethrin, making it an insecticide that is stable to air, moisture, and light [20]. Owing to its widespread use, the concentration of Deltamethrin in surface waters is high, owing to the lipophilicity of pyrethroids, They are difficult to remove from living organisms that endanger human health and the environment [21,22]. Deltamethrin can cause chronic diseases and has harmful effects on the nervous system, safety, and cardiovascular system, and cause genetic disorders, therefore, it has a long-term effect on mammals [23,24]. Today, the development of cost-effective, simple and rapid methods is an important challenge for the detection and removal of water-soluble contaminants [25]. There are various methods for removing pesticides from aqueous solutions, including biological treatments [26], membrane bioreactors [27], coagulation flocculation [28], catalytic reduction [29], photocatalytic degradation [30,31], and adsorption [32]. But many of these methods have constraint such as low flexibility in various conditions, high cost, low efficiency and harmful by-products. Adsorption is useful approach for decontamination of contaminated media [33,34]. Adsorption method is one of the methods used to remove various pesticides due to high efficiency and low cost [35–37]. The efficiency and cost of the adsorption process are strongly influenced by the adsorbent used, among the affordable adsorbents used are various adsorbents based on natural polymers such as chitosan, sodium alginate and carboxymethyl cellulose, because of their special factor groups they have are always considered [38–40]. On the other hands, magnetic nanoparticles high active surface is a very effective method can meliorate the efficiency of the adsorption process [41]. An important advantage is the use of magnetic nanoparticles in addition to improving the adsorbent efficiency, they can facilitate the separation of the adsorbent from aqueous solutions [42]. Therefore, in this study an adsorbent based on magnetic chitosan and polyacrylic acid (PAA) in the hydrogel format was synthesized and used for removal Deltamethrin from aqueous solution. So far, this adsorbent has not been investigated in any study for the removal of pesticides. In addition, the optimum condition for adsorption Deltamethrin by this adsorbent was investigated by used Response Surface Methodology. Hence, artificial neural networks are used to model intricate processes and validate the response surface model. Several isotherm and kinetic models were used to study the equilibrium, rate, and mechanism of the Deltamethrin pesticide adsorption process by CS/PAA/Fe_3O_4 nanocomposite hydrogel. Its thermodynamic study and the reusability of the adsorbent were studied to evaluate its potential for commercialization.

2. Material and methods

Chitosan(CS) with molecular weight: 100,000-300,000, iron (III) chloride($FeCl_3.6H_2O$), Iron (II) chloride ($FeCl_2.6H_2O$), Acrylic acid(AA), Methylenebisacrylamide (MBA) and Potassium persulfate (KPS), NaOH, Nitrate, Copper, and HCl were purchased from Merck Co (Germany). Deltamethrin (2/5 %) produced by Mahan Co was obtained from Iran. The pesticide Deltamethrin was diluted with distilled water to prepare a contaminant solution as the adsorption solution.

2.1. Synthesis of CS/PAA/Fe_3O_4

Synthesis of CS/PAA/Fe_3O_4 nanocomposite hydrogel was performed by copolymerization AA on the surface of CS-coated Fe_3O_4. Magnetic nanoparticles were synthesized by co-precipitation method Synthesis of magnetic nanoparticles was done by co-precipitation method using $Fe_3Cl_3.6H_2O$ and $Fe_3Cl_2.4H_2O$ in 2: 1 ratio, according to this study [43]. First, 0.5 g of CS to 25 mL of distilled water, then 255 μL of acetic acid was added to the solution to accelerate the dissolution of chitosan in water. Then 0.3 g of Fe_3O_4 was added to the solution and placed on a magnetic stirrer for 10 min until completely dispersed. Then, 1 mL of AA as a monomer and 0.024 g of MBA as a crosslinker were added to the solution simultaneously and stirred for 15 min. Finally, under a nitrogen atmosphere the polymerization and crosslinking were commenced by KPS at 70 ℃ for 60 min. The magnetic nanocomposite hydrogel obtained was isolated using an external magnetic field [44].

2.2. Characterization of magnetic nanocomposite hydrogel

Various analyzes have been used to investigate the surface properties and characteristics of CS/PAA/Fe_3O_4 nanocomposite hydrogel. FT-IR analysis (Broker victor 22) was used to identify CS/PAA, CS/PAA-delt, CS/PAA/Fe_3O_4, CS/PAA/Fe_3O_4-delt functional groups. XRD analysis to investigate the properties and crystal structure of the compounds synthesized materials were used (Philips PW 1730). Vibration sample magnetometer (VSM) analysis was used to investigate the magnetic properties of CS/PAA/Fe_3O_4 nanocomposite hydrogel and Fe_3O_4 nanoparticles. Thermal analysis (TGA) was performed on TGA instrument (TA, model Q600) at heating rate of 10 °C/min, from 25 to 1000 °C and argon atmosphere, in which changes in substance weight against temperature increase were measured to evaluate the structure and thermal stability of CS/PAA hydrogel and CS/PAA/Fe_3O_4 nanocomposite hydrogel. EDX, FE-SEM, and Map analysis were performed to investigate the structure, surface properties of the samples and to determine the composition of the elements in their structure, respectively.

2.3. Study of effective adsorption parameters

In this study, all adsorptions were performed discontinuously in 30 mL containers. To optimize the adsorption process to the situation pH parameters (3 to 11) (this range of pH includes acidic; alkaline and neutral.), initial concentration of Deltamethrin (20 to 100 mg/L) (the concentration of Deltamethrin in the environmental is more in this range.), time (30 to 150 min) (the time range was chosen so that the necessary opportunity for pesticide adsorption by the adsorbent is provided.), temperature (25 to 45 °C) (when the pesticides are used, the temperature of the aquatic environments under their influence is basically in this range.) and The amount of composite (0.5 to 2.5 g/L) (adsorbent dosage was selected according to the pesticide concentration range and other studies conducted.) on adsorption efficiency was checked to evaluate the adsorption process of Deltamethrin pesticide with CS/PAA/Fe_3O_4 nanocomposite hydrogel. The levels of the variables in the central composite design must be same intervals; in this study α value equal to 2 was considered for all variables. After each adsorption step, the adsorption of the magnetic composite is separated from the Deltamethrin solution using a magnet. Behind drying, its weight was measured.The adsorption capacity and efficiency of Deltamethrin pesticide were calculated by CS/PAA/Fe_3O_4 nanocomposite hydrogel adsorbent using the obtained results Eqs. (1), and (2).

$$q_e = (C_i - C_e) \times \frac{V}{m} \tag{1}$$

$$R(\%) = \left(\frac{C_i - C_e}{C_i}\right) \times 100 \tag{2}$$

Where R is adsorption percentage, q_e is the amount of adsorption at equilibrium (g/kg), C_e and C_i are the initial and equilibrium concentration of Deltamethrin (mg/L), respectively, V is the liquid volume (L) and m is the amount of adsorbent was used (g).

2.4. Designing experiments using (RSM-CCD)

Response Surface Methodology (RSM) was used to evaluate the optimal conditions for Deltamethrin removal [10,45]. RSM is a statistical method that is suitable for multifactorial experiments shows the

communication between different parameters for optimal effective situations [46,47]. In order to investigate the five parameters in 5 levels, the central composite design (CCD) was used Table 1. The number of experiments for the parameters of pH, elementary concentration of Deltamethrin temperature, adsorbent contact time, and the amount of composite consumed at the desired levels was obtained using the relation (2 k + 2 k + 4 = 46) where (k) the number of variables is independent using Design Expert 11 software. In this model, the variables are set at (−α, −1, 0, 1, + α) with four iterations at the center point.

The relationship between independent and dependent variables was obtained using Design Expert software .Then, using analysis of variance and *P*-value, significant and non-significant effects of independent variables determined was after removing the meaningless sum from the model and after modification, it was re-examined. The correlation coefficient (R^2) of the experimental results was compared with the results obtained from the RSM-CCD. Other suitable statistics such as (AP) adequate accuracy, (DF) desirability function, (CV %) coefficient of variation, and (SD) standard deviation were calculated by the software to evaluate the quality and efficiency of the model.

2.5. Adsorption and desorption of magnetic nanocomposite hydrogel

To reduce the costs of the Deltamethrin adsorption process by CS/PAA/Fe_3O_4 magnetic nanocomposite, adsorption and desorption of the adsorbent were studied. For this purpose, the adsorption process of Deltamethrin by the mentioned nanocomposite hydrogel was performed under optimal conditions. In desorption processes, solutions with different pHs are used. In the present study, the Briton-Robinson buffer was used for pH 1 to 13. Then, an adsorption test was performed and after separating the adsorbent from the solution and drying the adsorbent, desorption was performed in these buffers. Also, based on the percentage of desorption, the optimal pH was selected and the adsorption-desorption process under optimal conditions in the appropriate Britton-Robinson buffer was performed for up to 10 cycles and the percentage of desorption was calculated from Eq. (3).

$$\%\text{of Desorption} = \left(\frac{\text{amount of pesticide desorbed}}{\text{amount of pesticide adsorbed}}\right) \times 100 \quad (3)$$

2.6. Description of artificial neural network (ANN)

ANN nonlinear analytical method with unique performance is used to investigate different and complex models [48]. This study was used to model the adsorption of Deltamethrin by CS/PAA/Fe_3O_4 nanocomposite hydrogel for validation and comparison with the RSM-CCD artificial neural network method [49,50]. The output layer shows the percentage of adsorption. Eq. (4) was used to determine the number of hidden layers. In this Eq. (4), the upper bound and the lower bound are the numbers of variables and, the relationship is empirical respectively [51].

$$2(n_i + n_o) < n_1 < \frac{m(n_i + n_0) - n_o}{n_i + n_o + 1} \quad (4)$$

In this Eq. (4) n_i, n_o, n_1 and m are the numbers of inputs, outputs, hidden layer neurons, and available data, respectively. As well, error values of both using Eqs. (5) and (6) for Comparison of network performance with RSM equation were used.

$$MAE = \sum_{i=1}^{m} |(y_i - \widehat{y}_i)|/m \quad (5)$$

$$MAPE = \frac{100}{m} \sum_{i=1}^{m} \left(|y_i - \widehat{y}_i|/y_i\right) \quad (6)$$

$$RMSE = \sqrt{\sum_{i=1}^{m} (|\widehat{y}_i - y_i|)^2}/m \quad (7)$$

MAPE and MAE are average absolute percentand average absolute error, alThereforeRMSE is the root mean square error, $\widehat{y}_i$,y_i are the prediction and actual performance.

3. Result and discussion

3.1. Investigation of nanocomposite hydrogel

To investigate the chemical interaction and to identify functional groups in the CS/AA/Fe_3O_4 nanocomposite hydrogel before and after Deltamethrin adsorption FT-IR analysis was used (Fig. 1-a). The FT-IR spectrum of the synthesized CS/AA/Fe_3O_4 nanocomposite hydrogel has peaked at 1735 cm^{-1} and 1559 cm^{-1}, which corresponds to the C = O in the amide group and the N—H flexural vibrations, respectively. The peak of the 1066 cm^{-1} region belongs to the C—O tensile vibration group. In the area of 2850–3000 cm^{-1} corresponds to aliphatic C—H peaks, which appear here in the area of 2924 cm^{-1}, due to the large number of carbon atoms on the surface of chitosan. There is a strong adsorption peak in the 3438 cm^{-1} region due to the tensile vibrations of the O—H and N—H bonds in the chitosan structure in all FT-IR spectra [44]. AlThereforein the spectra where Fe_3O_4 is present, there is a peak of Fe—O in the region of 583 cm^{-1}, which indicates the peak of the magnetite index in the nanocomposite [52]. However, as can be seen in the spectra of CS/PAA and CS/PAA/Fe_3O_4 nanocomposite hydrogels, very different peaks are not visible after adsorption of Deltamethrin CS/PAA-delt, CS/PAA/Fe_3O_4-delt. According to FT-IR analysis and the obtained results, it can be concluded that the synthesis of nanocomposite hydrogel has been successful. VSM analysis was used to investigate the magnetic properties of Fe_3O_4 nanoparticles and synthesized CS/PAA/Fe_3O_4 magnetic nanocomposite hydrogel nanocomposite (Fig. 1-b). According to the diagram, no magnetic residues are observed in any of the curves. Furthermore; the diagrams of both materials are completely symmetric and pass through the origin of the coordinates, which indicates the lack of coercion and survival in the samples. These results indicate that Fe_3O_4 nanoparticles and CS/PAA/Fe_3O_4 magnetic nanocomposite hydrogels are superparamagnetic, therefor reusability and magnetic segregation are conceivable [53,54]. The magnetic saturation values of Fe_3O_4 nanoparticles and CS/PAA/Fe_3O_4 magnetic nanocomposite hydrogel are 84.36 emu/g and 11.33 emu/g, respectively. Placement of non-magnetic chitosan and polyacrylic acid matrices on the surface of CS/PAA/Fe_3O_4 magnetic nanocomposite hydrogel has reduced its magnetic saturation, which confirms the successful synthesis of this material [55]. Thermal analysis (TGA) was performed to evaluate the thermal properties of CS/PAA and CS/PAA/Fe_3O_4 nanocomposite

Table 1
Independent variables in the experiments.

Independent variables	Coded	Unit	Factorial and center level			Axial level	
			Low (−1)	Center (0)	High (+1)	Lowest (−α)	Highest (+α)
pH value	X_1	–	5	7	9	3	11
Deltamethrin concentration	X_2	mg/L	40	60	80	20	100
time	X_3	min	60	90	120	30	150
dosage	X_4	g/L	1	1.5	2	0.5	2.5
Temperature	X_5	C·	30	35	40	25	45

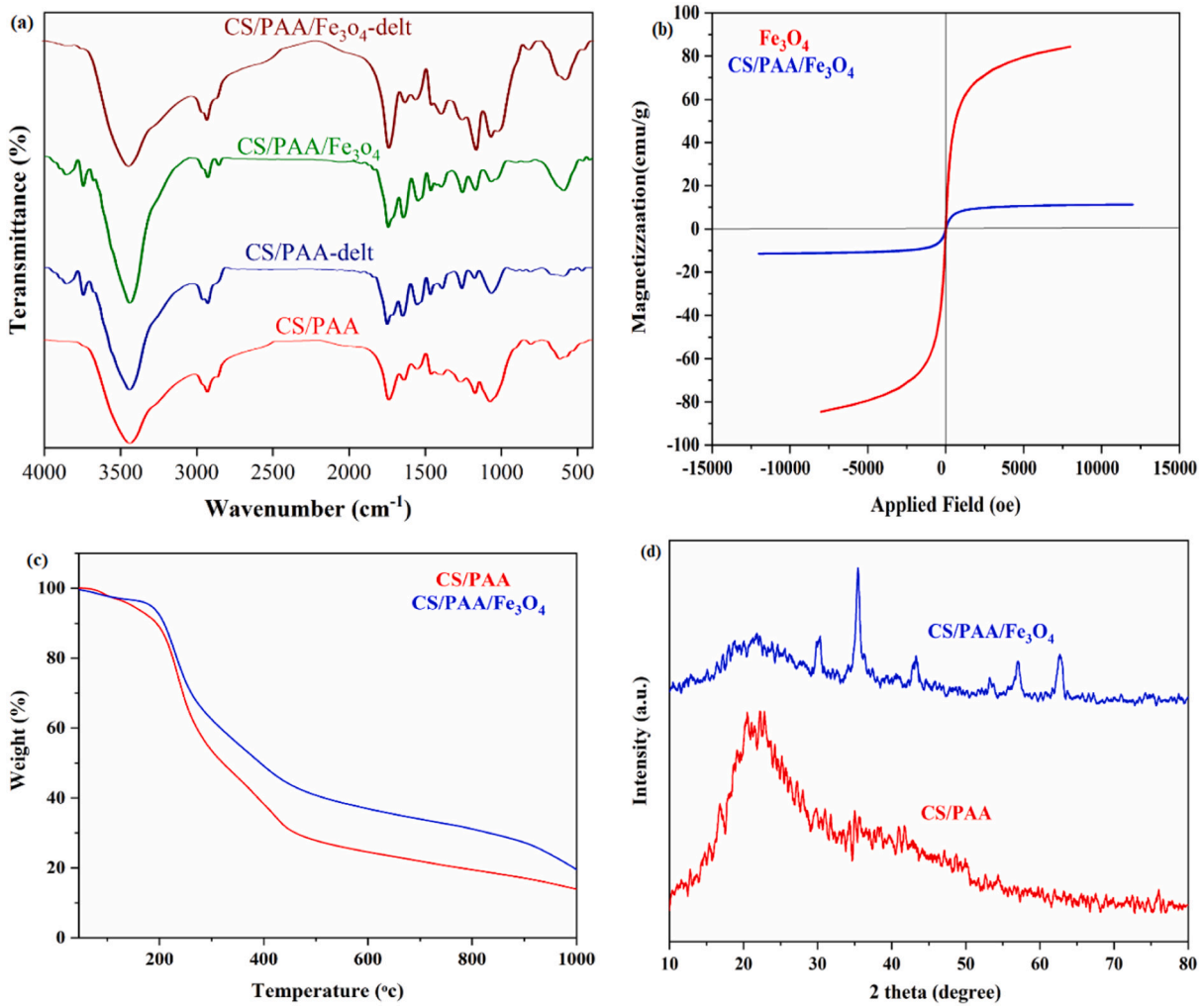

Fig. 1. (a) FTIR spectrum, (b) VSM analysis of Fe_3O_4 and CS/PAA/Fe_3O_4, (c) TGA curve of the CS/PAA and CS/PAA/Fe_3O_4 and, (d) XRD pattern.

hydrogels (Fig. 1-c). As can be seen, in the temperature range of 40 to 1000 ℃, three different weight loss stages can be seen in the diagram related to both samples. In the temperature range of approximately 40 to 200 ℃, 10 % and 15 % for CS/PAA and CS/PAA/Fe_3O_4 are observed in the graphs for both materials, respectively, which are related to the loss of water in their structure at this temperature. The second stage of severe weight loss of 45 % and 40 % by weight for CS/PAA and CS/PAA/Fe_3O_4 nanocomposites in the temperature range of 200 to 400 ℃, respectively, is related to the degradation of chitosan polymer and polyacrylic acid carboxylate groups [52,56]. The third stage of weight loss due to temperature increase and finally weight loss of CS/PAA and CS/PAA/Fe_3O_4 in the temperature range of 400 to 850 ℃ is related to the failure of polyacrylic acid polymer chains and hydroxylation of Fe_3O_4 nanoparticles at high temperatures [52,57]. Also, the temperature resistance and burnt residue for CS/PAA/Fe_3O_4 are higher than CS/PAA, which can be due to the thermal stability of magnetite nanoparticles up to 596 ℃ [52]. XRD analysis was performed to investigate the structure of CS/PAA and CS/PAA/Fe_3O_4 nanocomposite hydrogels in the range of 20 to 80 degrees and the results are shown in (Fig. 1-d). As can be seen in the XRD spectrum of CS/PAA hydrogels a wide peak is observed at 2θ values of 36.22° which is produced by polyacrylic acid which indicates that CS/PAA is amorphous [58]. It is alThereforeobserved that the existing wide peak has two peaks which are due to chitosan in the structure of the mentioned hydrogel [59]. This spectrum generally indicates that the hydrogel has an almost amorphous structure [52]. In the XRD spectrum of the CS/PAA/Fe_3O_4 nanocomposite hydrogel, a wide peak is observed, which is alThereforevisible in the CS/PAA structure. AlThereforein the CS/PAA/Fe_3O_4 nanocomposite hydrogel structure, other peaks are observed in the regions 2θ (°) equal to 30.34, 35.44, 43.26, 53.18, 57.02, and 62.68. This corresponds to crystal plates with Miller index equal to (220), (311), (400), (422), (511) and (440), respectively [53]. The six peaks discussed are due to Fe_3O_4 nanoparticles in the CS/PAA/Fe_3O_4 nanocomposite hydrogel structure. In addition, the presence of these peaks indicates the semi-crystalline structure of CS/PAA/Fe_3O_4 nanocomposite hydrogel. Therefore, the size of the crystals for the mentioned nanocomposite hydrogel was calculated using the Debye Scherrer relationship. The results show that the distance between the crystal plates and the size of the crystals is 0.253 nm and 43.2 nm, respectively.

Fig. 2 compares CS/PAA hydrogel with CS/PAA/Fe_3O_4 nanocomposite hydrogel.This confirms the successful placement of Fe_3O_4 nanoparticles on the surface of the relevant nanocomposite hydrogel. As can be seen, the surface of the hydrogel is uneven and has cavities that are covered by Fe_3O_4 particles in the nanocomposites hydrogel. In other words, iron nanoparticles were placed on the surface of the CS/PAA hydrogel. This confirms the successful synthesis and prosperous placement of Fe_3O_4 nanoparticles on the surface of the respective nanocomposite hydrogel.

FE-SEM, EDX, and Map analyses to investigate the nanoparticle morphology, percentage of elements and dispersion of nanoparticles related to CS/PAA/Fe_3O_4 nanocomposite hydrogel before and after Deltamethrin adsorption are shown in Fig. 3, respectively. FE-SEM analysis shows the surface of the nanocomposite hydrogel before

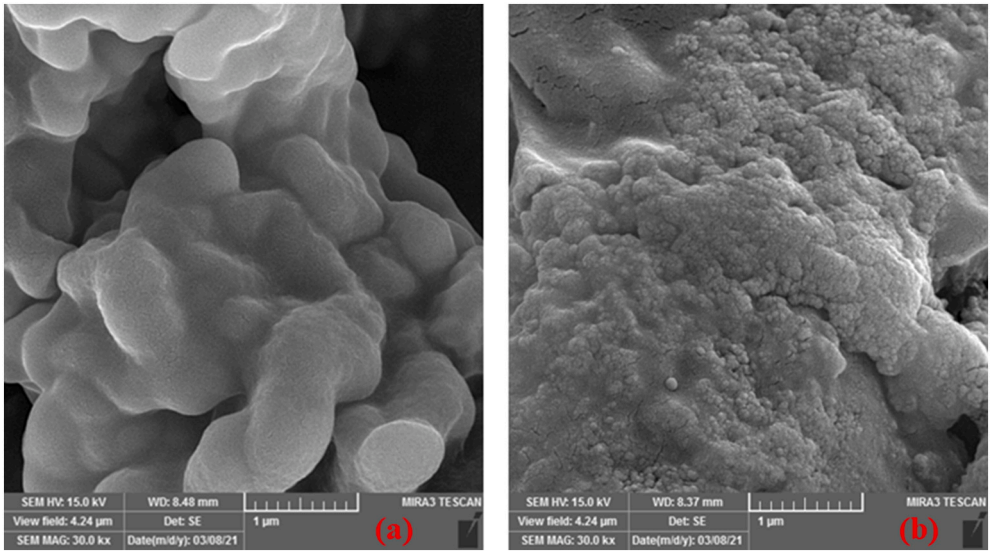

Fig. 2. Analysis FE-SEM CS/PAA hydrogel (a) and CS/PAA/Fe_3O_4 nanocomposite hydrogel (b).

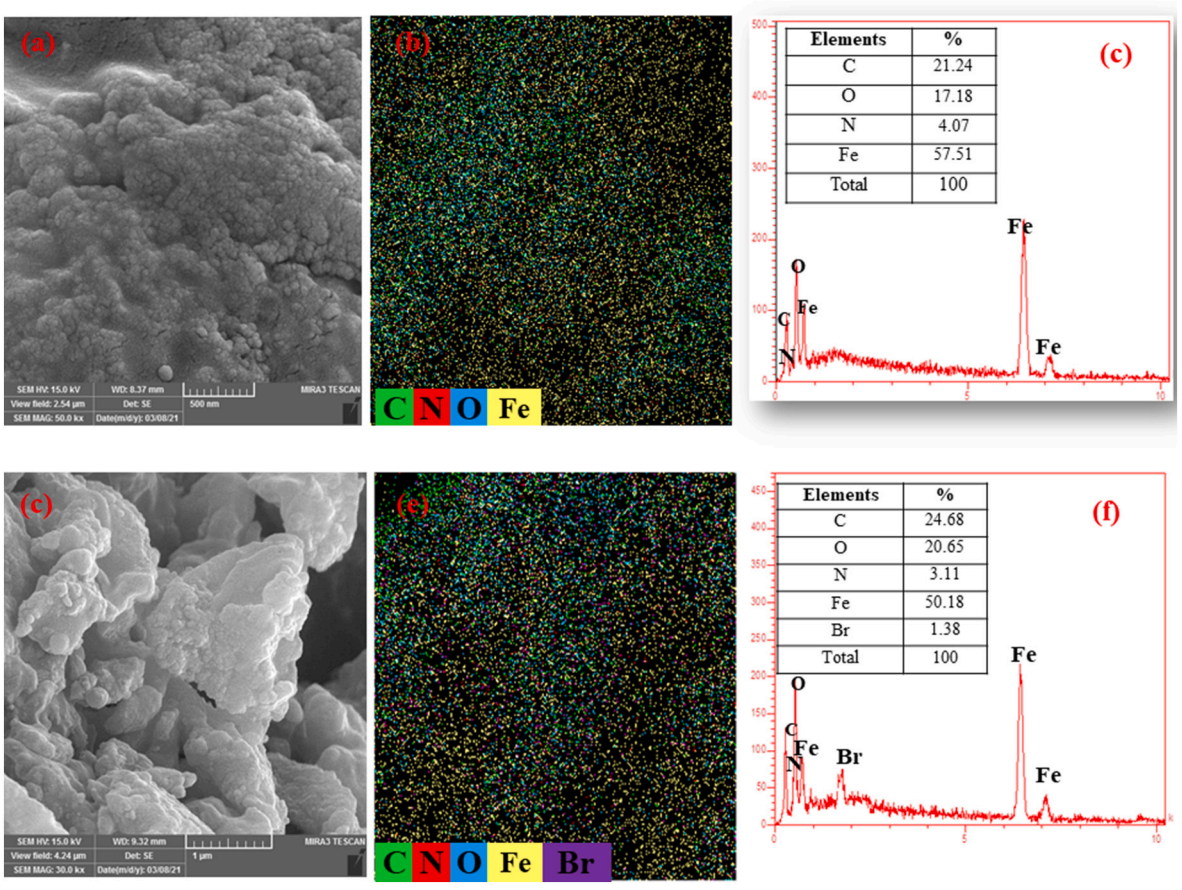

Fig. 3. FE-SEM test for a) CS/PAA/Fe_3O_4, b) CS/PAA/Fe_3O_4-delt and Map-EDX test for CS/PAA/Fe_3O_4 (b,c) and CS/PAA/Fe_3O_4-delt (e,f).

adsorption of Deltamethrin in addition to having a rough surface and cavities related to CS/PAA. Also, CS/PAA are covered with a coating of Fe_3O_4 that is fully visible (Fig. 3-a). In addition, the results of Map and EDX analysis show that iron nanoparticles are located on the surface of this hydrogel and are evenly distributed and the highest percentage of elements is related to Fe (Fig. 3-b, c). Also, after adsorption of Deltamethrin by CS/PAA/Fe_3O_4, it is observed that the surface of the hydrogel is completely covered by the toxin particles (Fig. 3-d). The results of Map analysis and EDX alThereforeshow the uniform placement of Deltamethrin on the surface of the nanocomposite hydrogel (Fig. 3-e, f).

3.2. Results of Response Surface Methodology (RSM-CCD)

In order to obtain a suitable model for predicting and optimizing experimental data and designing logical experiments and analyzing the interactions between the parameters, the response surface methodology (RSM) and central composite design (CCD) were used [46,47]. Experimental designs can have a significant impact on estimated accuracy as well as adsorption costs [60,61]. In the first step, the assumption of data normality was examined. For this purpose, the normal distribution diagram, residual value diagram versus the number of experiments, residual studentized diagram versus predicted values and box-cox were extracted. Due to the normal distribution diagram, most of the experimental data are concentrated around the line and are not the "S" pattern. The residual studentized diagram alThereforehas not the ">"pattern. On the other hand, in Box-Cox chart, the best lambda amount is 0.56, which is in the 95 % confidence range of 0.88 to 0.23, from these three graphs, it can be concluded that the data are normal [62].

In the second stage, the obtained model was examined and then the model was modified and meaningless sentences were removed (8). In this equation variables, X_5, X_4, X_3, X_2, and, X_1 are equivalent to temperature, hydrogel value, contact time, the primary concentration of Deltamethrin, and pH respectively, and its R^2 is equal to 0.988. Due to the proximity of the data to the average amount and their low dispersion, shows the validity of the data, alThereforebecause of the low value of the coefficient of variation (<10 %), it can be concluded that the model is reproducibility [63]. On the other hand, the correlation coefficient related to the prediction of the model was 0.9987, as a result, the model has a high ability to predict data and the data from the experiments are very close to the data estimated by the model (Fig. 4).

The appropriate accuracy value (AP) indicates the noise signal rate, which was calculated to be 243.66, because the AP is much larger than 4, indicating the suitability of the model [64,65]. To design the connection between adsorption efficiency and selective factors, alThereforethe effect of changing the first and second power of the variable on the adsorption efficiency was investigated using Eq. (8). But this equation does not provide enough information about the nature and the intensity of the effect of each variable.

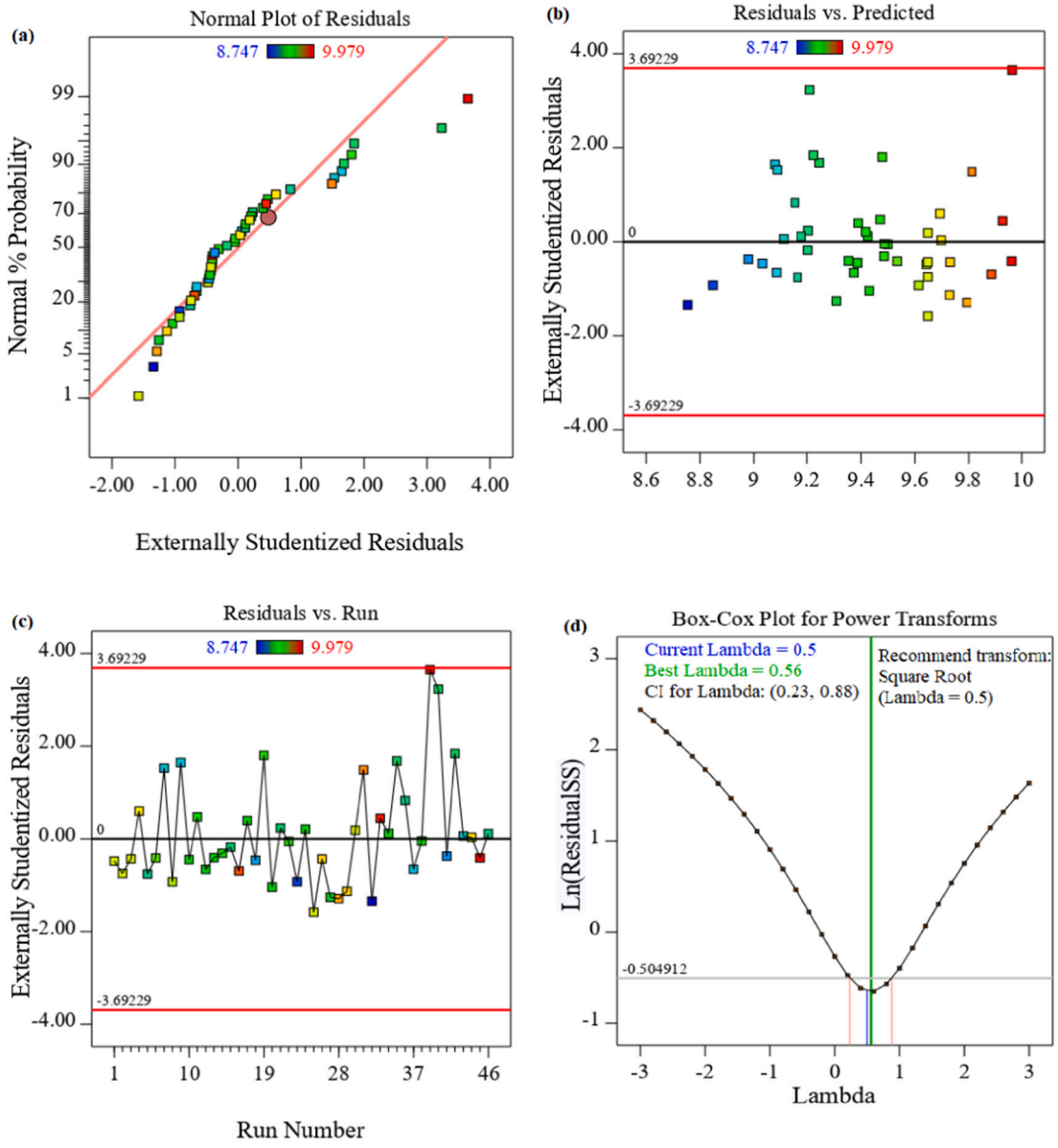

Fig. 4. a) Normal distribution diagram, b) Externally studentized against the foretoken amount, c) Residuals Residuals against run number, d) Box-Cox diagram.

$$R = 6.25 + 0.46X_1 - 0.018X_2 - 0.006X_3 - 0.62X_4 + 0.05X_5 + 4.7 \times 10^{-5}X_1X_2 + 4.96 \times 10^{-4}X_1X_3 + 0.017X_1X_4 + 0.001X_1X_5 - 2.2 \times 10^{-5}X_2X_3 + 1.84 \times 10^{-4}X_2X_4 - 4.4 \times 10^{-5}X_2X_5 - 8.5 \times 10^{-5}X_3X_5 + 2.24 \times 10^{-3}X_4X_5 + 0.03X_1^2 + 1.01 \times 10^{-4}X_2^2 + 2.7 \times 10^{-5}X_3^2 - 0.078X_4^2 + 0.001X_5^2 \quad (8)$$

After removing the Non-meaningful sentences, the results of the analysis of variance (ANOVA) for the Deltamethrin adsorption process by CS/PAA/Fe_3O_4 nanocomposite hydrogel were studied (Table 2). According to the table (ANOVA), the *p*-value is <0.0001, indicating that the model is significant at the 99 % level. In addition, the lack-of-fit value is non-significance, which indicates that the obtained model has the ability to predict process efficiency. Variables that have a significant interaction are listed in Table 2 and Eq. (8). But this equation does not provide enough information about the nature and the intensity of the effect of each variable. For this reason, the Perturbation diagram (Fig. 5) in which the effect of each of the independent variables the following is explained.

In Fig. 5 As can be seen, CS/PAA/Fe_3O_4 nanocomposite hydrogel has an effect on pH, time, and temperature variables as a curve and In Eq. (8), there is a quadratic power of all of them [66]. The effect of increasing temperature alThereforereduces the adsorption efficiency, which can be due to increased mobility of Deltamethrin, shrinkage, and change in active sites at the nanocomposite surface at high temperatures. The reason for this is the tendency of the adsorbed toxins to separate from the active sites of the adsorbent and be released into the solution and reduce the active surface of the nanocomposite [67]. It is alThereforeobserved that with increasing contact time, the efficiency of the Deltamethrin adsorption process by CS/PAA/Fe_3O_4 nanocomposite hydrogel increases due to having enough time to place Deltamethrin on the surface of active nanocomposite sites, but it has remained stable due to the saturation of available empty sites [68,69]. The effect of increasing the primary concentration of Deltamethrin on the adsorption efficiency is decreased, which can be due to the increase in the initial concentration of Deltamethrin on the adsorbent surface, resulting in saturation of active sites in the surface becomes adsorbent, which reduces the adsorption efficiency of pesticides at high concentrations. As well as, the results showed that with incrementing the amount of nanocomposite hydrogel due to increasing the number of active sites on the adsorbent surface, the amount of adsorption efficiency increases. According to Fig. 5, the pH variable diagram is curved and shows the highest adsorption efficiency of Deltamethrin by the mentioned

Table 2
Quadratic ANOVA analysis model for Deltamethrin removal.

Source	Df[a]	SS[b]	MS[c]	F-value	P-value
Model	19	4	21.08×10^{-2}	3720.17	<0.0001
X_1	1	7.04×10^{-2}	7.04×10^{-2}	1241.93	<0.0001
X_2	1	38.55×10^{2}	38.55×10^{-2}	6803.52	<0.0001
X_3	1	74.63×10^{2}	0.7463	13,171.54	<0.0001
X_4	1	1.29	1.29	22,770.91	<0.0001
X_5	1	0.8685	0.8685	15,328.18	<0.0001
X_1 X_2	1	0.0003	0.0003	4.55	0.0425
X_1X_3	1	0.0126	0.0126	222.1	<0.0001
X_1X_4	1	0.0095	0.0095	168.11	<0.0001
X_1X_5	1	0.0033	0.0033	57.67	<0.0001
X_2X_3	1	0.0056	0.0056	99.65	<0.0001
X_2 X_4	1	0.0002	0.0002	4.3	0.0482
X_2X_5	1	0.0014	0.0014	24.33	<0.0001
X_3X_5	1	0.0023	0.0023	40.36	<0.0001
X_4X_5	1	0.001	0.001	17.66	0.0003
X_1^2	1	0.4089	0.4089	7217.85	<0.0001
X_2^2	1	0.2303	0.2303	4064.36	<0.0001
X_3^2	1	0.0032	0.0032	56.8	<0.0001
X_4^2	1	0.0106	0.0106	187.83	<0.0001
X_5^2	1	0.0288	0.0288	187.83	<0.0001
Residual	26	0.0015	0.0001	–	–
Lack of Fit	23	0.0014	0.0001	2.72	0.2233
Pure Error	3	0.0001	0.0000	–	–
Cor Total	45	4.01	–	–	–

Model summary statistics

Response	Std. Dev. (SD)	Coefficient of Variance (C. V. %)	R^2	Adj-R^2	Pred-R^2	AP[d]
R%	0.0075	0.0798	0.9996	0.9994	0.9986	243.659

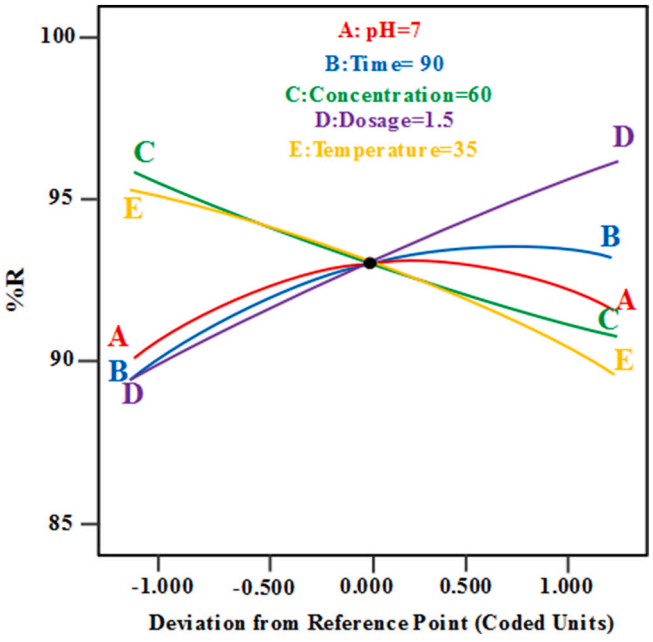

Fig. 5. Perturbation graph for all factors in center poin.

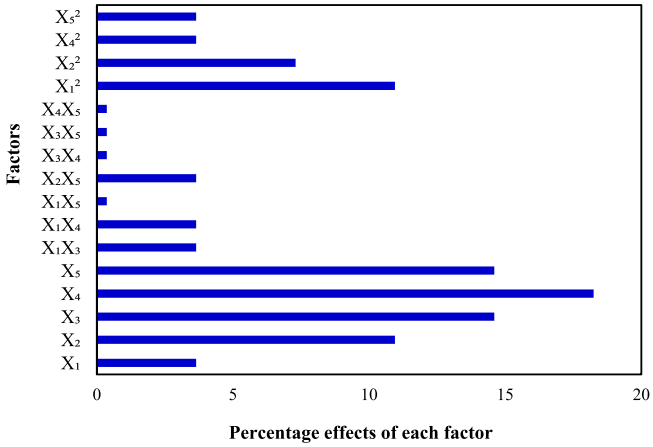

Fig. 6. Pareto chart for all significant factors.

hydrogel nanocomposite in neutral environments [70,71]. Due to the uncertainty of the effect of significant variables on each other and the sensitivity of its response is visible only to the independent variables and also, the extent to which the interactions are effective is not recognizable. Therefor a Pareto diagram was examined Fig. 6 [72]. The horizontal axle shows the percent effect of each parameter in the Parthenon diagram. According to Fig. 6, mixing pH with temperature has the least effect and the first power of the amount of nanocomposite hydrogel shows the greatest effect (Table 2).

In the next step, three-dimensional graphs were used to investigate the simultaneous effect of two parameters in situations where other variables have a fixed value Fig. 7 [72].Fig. 7a the effect of pH and time variables is investigated. The maximum adsorption efficiency is at pH 7 and the time efficiency is 90 to 120 min. The reason for the low adsorption efficiency at low pHs can be attributed to the presence of H^+ ions at these pHs and their competition with the cationic charge in Deltamethrin molecules for placement on the adsorbent surface. Therefore, the lower the concentration of H^+ or OH^- ions in the solution, the higher the rate of toxin removal in the solution, and alTherefor-eincreases the adsorption amount by increasing the contact time of the adsorbent with the toxin ions. The increase in adsorption percentage occurs due to more contact of Deltamethrin with the adsorbent and eventually reaches the maximum value. However, with increasing contact time due to saturation of empty sites, the amount of adsorption remains almost constant. Fig. 7b the effect of pH variables and primary concentration of Deltamethrin on it is adsorption efficiency shows that at pH equal to 7 and primary concentration of toxin approximately equal to 20 mg/L had the highest efficiency. Fig. 7c the interaction of two pH parameters and the amount of composite is investigated. The maximum efficiency at neutral pH and the amount of composite is 2.5 g/L, which increases the number of active adsorbent sites, and increases the adsorption of Deltamethrin. Fig. 7d the effect of temperature and pH variables on the efficiency of Deltamethrin uptake is shown. Which shows the highest efficiency at pH 7 and a temperature of 25 °C. Fig. 7e shows the interaction of primary Deltamethrin concentration and time, the highest adsorption rate at the primary concentration of 10 mg/L and a time of 100 min, which is called the equilibrium time, then remained constant due to the filling of active sites. Fig. 7f the interaction of the variables shows the amount of composite and contact time, in which the adsorption efficiency increases with the increase of these two variables. Fig. 7g examined the simultaneous effect of time and temperature, which shows the highest efficiency at 25 °C and 100 min. Fig. 7h indicates the interaction of primary concentration and temperature variables. These two variables are a plate with a negative slope for concentration and temperature, which decreases with increasing concentration due to the increase of pollutant molecules. Fig. 7i shows the interaction between the amount of composite and the temperature. As can be seen in the figure, the increase in temperature is inversely related

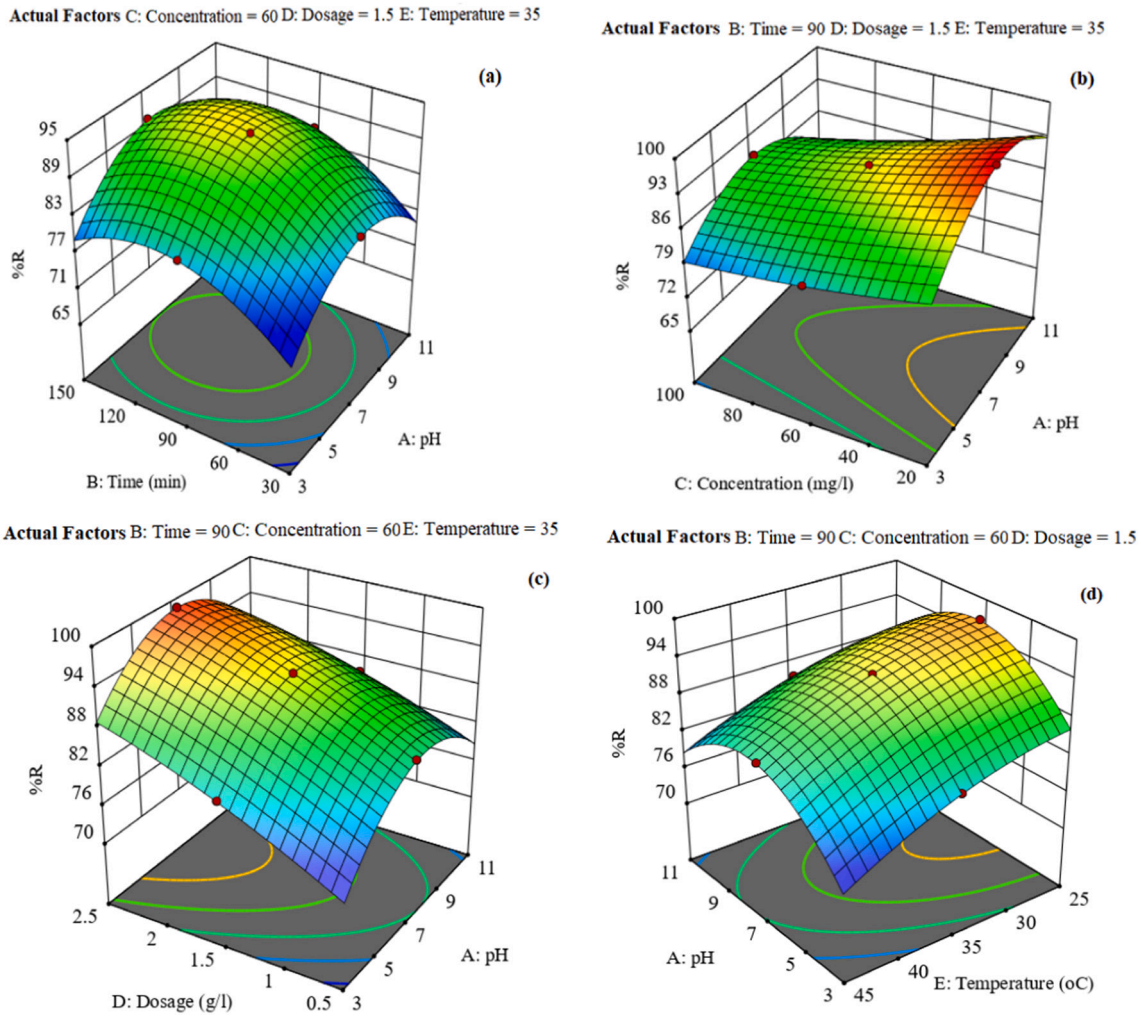

Fig. 7. Diagrams of interactions a) time and pH, b)concentration of Deltamethrin and pH, c) amount of composite and pH, d)Temperature and pH, e) time and concentration of Deltamethrin, f) time and amount of composite, g) time and Temperature, h) Temperature and concentration of Deltamethrin, i) Temperature and amount of composite.

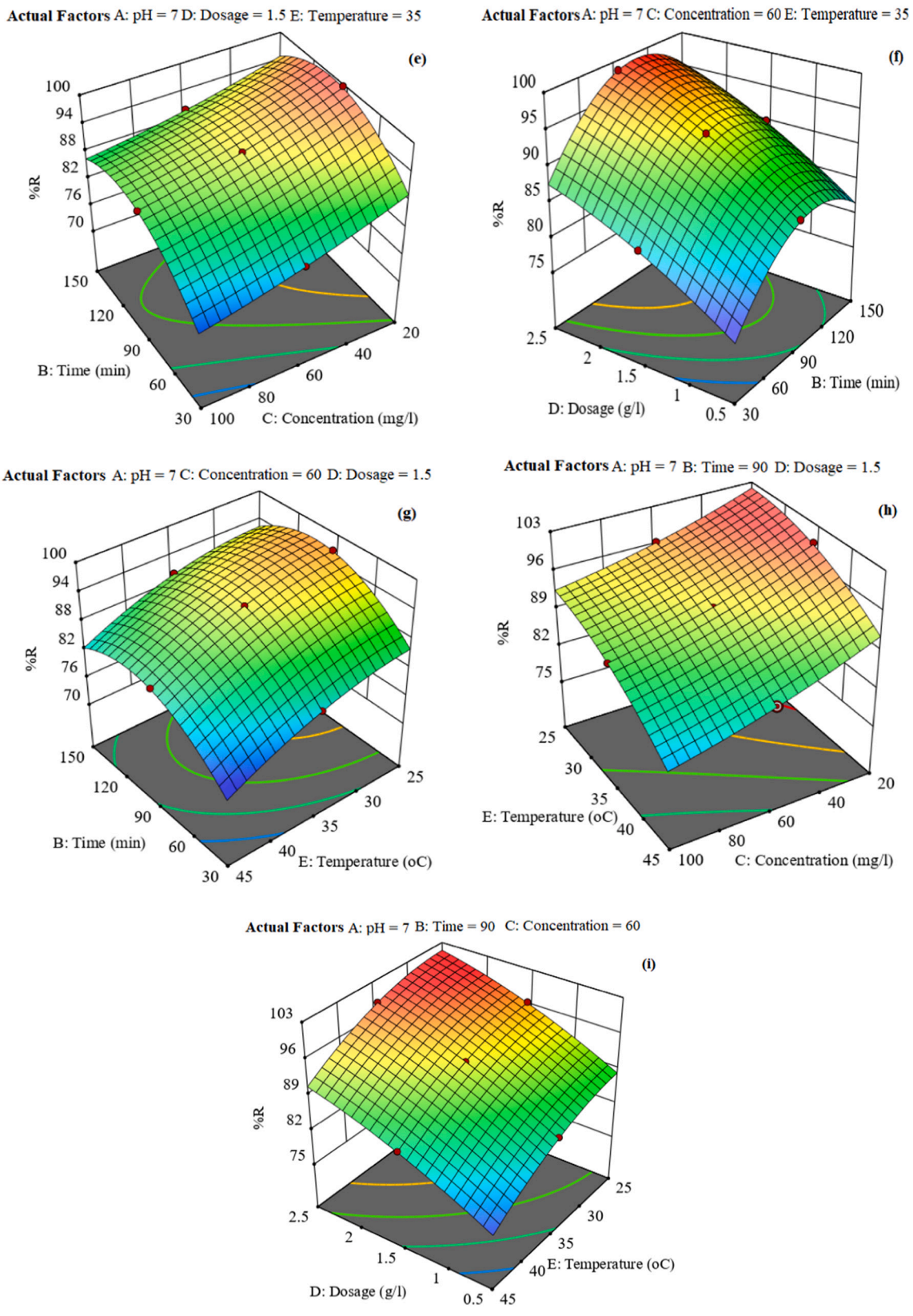

Fig. 7. (*continued*).

to the percentage of adsorption, thus the maximum amount of adsorption at the initial temperature of 25 °C and the amount of composite is 2.5 g/L.

Since three-dimensional diagrams cannot have enough information about the general optimal conditions, the optimization of variables was examined to determine the appropriate conditions for having the highest adsorption efficiency Fig. 8. As can be seen, the highest efficiency of Deltamethrin uptake by CS/PAA/Fe_3O_4 nanocomposite hydrogel was

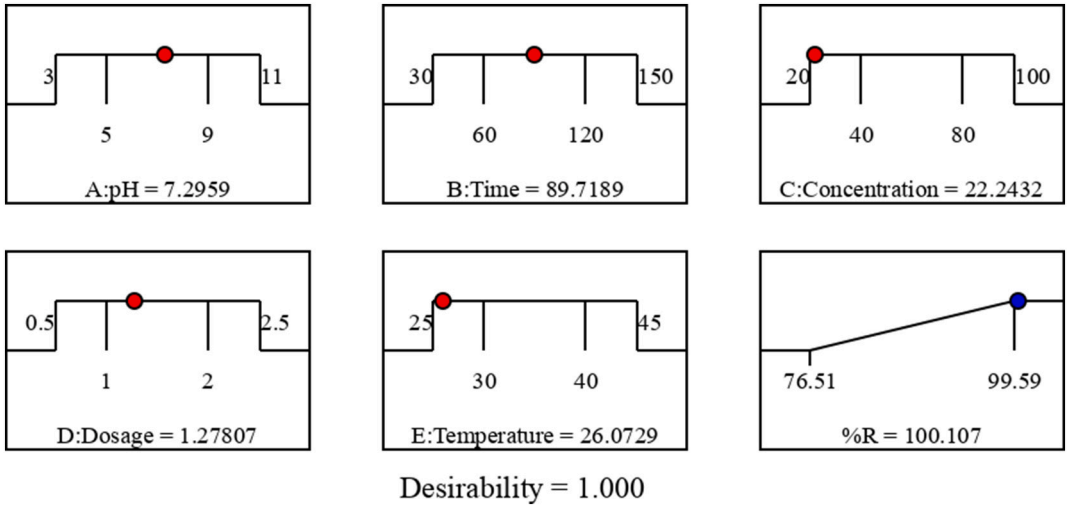

Fig. 8. Actual profiles with optimal performance prediction points for Deltamethrin removal by CS/PAA/Fe_3O_4 nanocomposite hydrogel.

100.1 % at a temperature of 26/07 °C, initial concentration of 22/24 mg/L, contact time equal to 89.72 min, the adsorbent dose is 1.28 g/L and the neutral pH. This indicates the high ability of nanocomposite to adsorb Deltamethrin. To further investigate the optimal adsorption conditions, an experimental experiment was performed under these conditions and its efficiency was calculated to be equal to 99.79 %. The little difference between the maximum value of the experimental adsorption percentage and the model adsorption percentage indicates the CCD model's suitability for optimizing the Deltamethrin adsorption process by the CS/PAA/Fe_3O_4 nanocomposite hydrogel [73]. Also, the real sample of river water (COD: 198 mg O_2/L) with 20 ppm of Deltamethrin was process in optimum condition. Removal percentage in the adsorption process of real sample is equal to 91.24 %. This result shows the high adsorption efficiency of CS/PAA/Fe_3O_4 in real samples. Also, the concentration of Fe^{3+} ion in real sample after adsorption process was measured to evaluate the leaching value. The concentration of Fe^{3+} ion is <1 ppm. The CS/PAA/Fe_3O_4 nanocomposite hydrogel is based on chitosan and the iron nanoparticles inside it are coated with chitosan, this material is stable in neutral environments and does not undergo leaching. Therefore, the concentration of Fe^{3+} ion concentration in optimal conditions for the adsorption process is very low.

3.3. Equilibrium study

The equilibrium study reveals important information about the distribution of adsorbent molecules in the liquid phase at equilibrium [74].

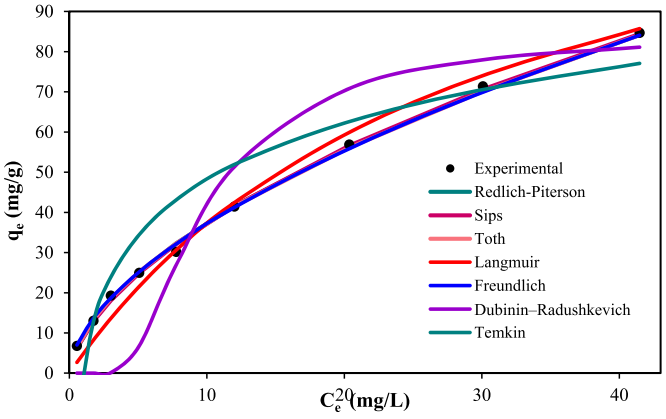

Fig. 9. Graphs of isotherm for CS/PAA/Fe_3O_4 nanocomposite hydrogel.

To examine the equilibrium study under optimal conditions where the parameters of pH, contact time, composite amount, and temperature are constant, isothermal models that show the connection between the amount of material adsorbed by the CS/PAA/Fe_3O_4 nanocomposite hydrogel and the residue in solution were examined. For this purpose, Two-parameter and three-parameter models such as Freundlich (used for adsorbents with uneven surfaces in the constant concentration range), Langmuir, Temkin, Dubinin-Radushkevich, and Sips, Toth and Redlich-Peterson respectively, were studied (Fig. 9 and Table 3). The model with the highest R^2 and the lowest mean root error will be suitable as a model. The values of R_L, n, and E parameters were 0.824–0.189, 1.335, and (0.233KJ/mol) based on two-parameter models, which indicate the desirability and physicality of the adsorption process. On the other hand, the three-parameter models Toth, Sips, and Redlich-Peterson are more suitable models due to their higher R^2. Among the three-parameter models, the coefficient of determination (R^2) and the root mean square error (RMSE) of all three models are equal. However, considering the values of a_T and a_S coefficients of the Toth and Sips models, these coefficients have very small values that can be ignored. Therefore the best model in the equilibrium study for the adsorption of deltamethrin using CS/PAA/Fe_3O_4 nanocomposite hydrogel is the Freundlich model [75].

3.4. Study of adsorption kinetics

To study the different times for the completion of the adsorption process and its speed to study the kinetics of the process. Also, adsorption kinetics provide useful information about understanding the mechanism of the adsorption process [76]. The kinetic study was performed at various times and at optimal pH, temperature, concentration, and adsorbent dose. In order to determine the appropriate kinetic model for Deltamethrin adsorption using CS/PAA/Fe_3O_4 nanocomposite hydrogel, the Elovich, pseudo-first and second-order kinetic models were investigated. The information obtained from the study of kinetic models can be used to design and model the adsorption processes based on the root mean square error of the coefficient of determination and the ability to explain the ability of each of these models Table 4. The results obtained from the study of these models showed that the adsorption process follows a second-order kinetic models. Therefore, it can be derived that the adsorption process using the nanocomposite hydrogel is based on chemical reactions Which expresses this there is an exchange of electrons between the adsorbent surface and the adsorbent [76]. The primary adsorption rate (h) was determined and its value was 4.17 (Fig. 10).

Table 3
Different models and parameters of two-parameter and three-parameter isotherms.

Models	Parameters	Analyte	R^2	RMSE
Langmuir	q_m(mg/g)	369.9		
$q_e = \frac{q_m k_L C_e}{1 + k_L C_e}$	k_L (L/mg)	0.0214	0.975	7.27
$R_L = \frac{1}{1 + k_L C_t}$	R_L	0.824–0.189		
Freundlich	n	1.335		
$q_e = k_f C_e^{1/n}$	k_f ((mg/g).(L/mg)$^{1/n}$)	11.6	0.983	5.705
Dubinin–Radushkevich (D-R)	E (KJ/mol)	0.233		
$q_e = q_m exp\left(-\beta\left(RT\, ln\left(1 + \left(1/C_e\right)\right)\right)^2\right)$	q_m (mg/g)	124.6	0.867	16.14
$E = \frac{1}{\sqrt{2\beta}}$	βx10^{-6}(mol^2/J^2)	9.17		
Temkin	B	30.79		
$q_e = B\, ln(A_T C_e)$	A_T(L/g)	111.9	0.556	29.49
Redlich-Peterson	k_{rp}(L/g)	39,620		
$q_e = \frac{k_{rp} C_e}{1 + \alpha_{rp} C_e^{\beta_{rp}}}$	α_{rp}(L/mg)$^{\beta rp}$	3.04		
	β_{rp}	342	0.983	6.1
Sips	k_s(L/mg)^{ms}	11.6		
$q_e = \frac{k_s C_e^{m_s}}{1 + a_s C_e^{m_s}}$	m_s	0.75		
	a_s(L/mg)^{ms}	5.85 × 10^{-11}	0.983	5.705
Toth	k_T(mg/g)	11.6		
$q_e = \frac{k_T C_e}{(a_T + C_e)^{1/t}}$	a_T(mg/g)	5.83 × 10^{-10}		
	T	3.986	0.983	5.705

qe: The amount of Deltamethrin adsorbed on the adsorbent (mg/g), k_L: energy of adsorption, Ce: concentration of Deltametrin in equilibrium time (mg/L), R_L: separation factor, E: average free energy of adsorption, qm: Maximum adsorption capacity, K_f: The amount of Deltamethrin adsorbed at a given concentration, A_T: Equilibrium constant related to connection energy, β: Adsorption energy constant, n: measurement of adsorption severity, t, k_T and a_T: Toth isotherm constants.

Table 4
kinetic model pseudo-first-order, pseudo-second-order, and Elovich kinetic diagrams.

Kinetic model	Parameters	Analyte
Pseudo-first- Order	$q_{e.\ Cal}$(mg/g)	7.342
	k_1(1/min)	0.1899
$q_t = q_e(1 - e^{-k_1 t})$	R^2	0.906
	RMSE	0. 113
Pseudo-second-order	$q_{e.\ Cal}$(mg/g)	7.55
	k_2(g/mg.min)	0.73
$q_t = \frac{k_2 q_e^2 t}{1 + k_2 q_e t}$	R^2	0.967
	RMSE	0.0671
$h = k_2 q_e^2$	h(mg/g.min)	4.1673
Elovich	α(mg/g.min)	6.39 × 10^{+8}
	β(g/mg)	0.312
$q_t = \beta\, \ln(\alpha\beta t)$	R^2	0.717
	RMSE	0.195
	$q_{e.exp}$(mg/g)	7.41

q_e: Adsorption valence equilibrium time (mg/g), t: contact time (min) and q_t: Adsorption valence in t, $k_1$and k_2: Pseudo-first and second-order rate constant, β: adsorption constant, h and α: primary adsorption rate.

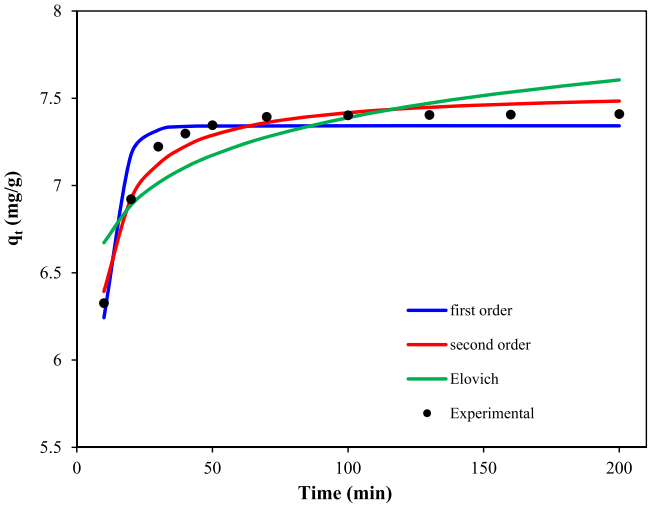

Fig. 10. Kinetic graphs Elovich, pseudo-first and second-order.

3.5. Study of adsorption mechanism for Deltamethrin removal

In order to study the adsorption mechanism of Deltamethrin by CS/PAA/Fe_3O_4 nanocomposite hydrogel, models of intraparticle diffusion, double-exponential, and liquid film diffusion were investigated Fig. 11. Due to the fact that in the particle diffusion model, the width value is positive from the origin and does not have a good value, it indicates the effect of a mechanism other than intraparticle diffusion on the adsorption. Therefore, the intraparticle diffusion model is not suitable for expressing the adsorption process of Deltamethrin by CS/PAA/Fe_3O_4 nanocomposite hydrogel [77]. That is, in addition to the intraparticle diffusion mechanism, another mechanism probably controls the toxin uptake process. The double-exponential model was recognized as a suitable model for describing the Deltamethrin adsorption process using the mentioned nanocomposite hydrogel due to having the highest amount of R^2 and the lowest amount of RMSE (Table 5). This model includes two stages of fast and slow penetration; it is related to the diffusion of inter-particle and intra-particle penetration, respectively [75]. The speed values for the fast (k_1) and slow (k_2) stages are 10.55 and 0.083 per min, respectively.

3.6. Thermodynamics of adsorption

Thermodynamic studies are used to evaluate the desirability of the Deltamethrin adsorption process by CS/PAA/Fe_3O_4 nanocomposite hydrogel. For this purpose, Thermodynamic parameters, including Gibbs free energy (ΔG°), enthalpy (ΔH°), and entropy (ΔS°) were examined; these three parameters have a very important impact on a better understanding of the adsorption process [78]. In this study, in optimal conditions, temperatures of 25 to 50 were used to determine the

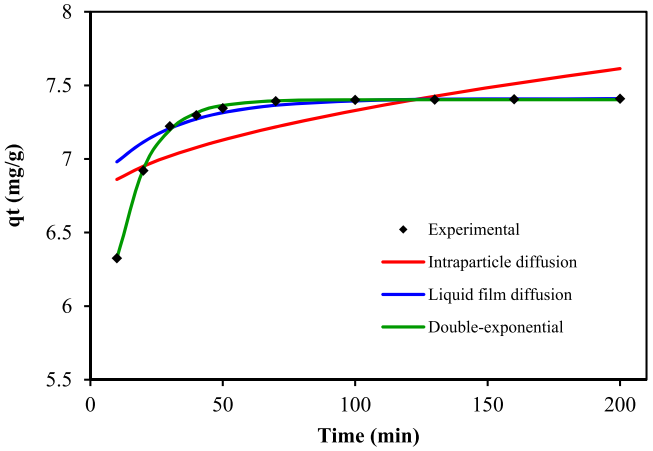

Fig. 11. Diagrams of the mechanism of adsorption related to the uptake of Deltametrin by CS/PAA/Fe_3O_4 nanocomposite hydrogel.

Table 5
Adsorption mechanism models and their parameters related to Deltamethrin adsorption.

Mechanism model	Parameters	Concentration (mg/L)
Intraparticle diffusion	k_{id}(1/m in)	0.069
	C (mg/g)	6.644
$q_t = k_{id}t^{1/2} + C$	R^2	0.524
	RMSE	0.253
Liquid film diffusion	k_{fd}(1/min)	0.038
	R^2	0.896
$\ln(1-(q_t/q_e)) = -k_{fd}t$	RMSE	0.711
Double-exponential	k_1(1/min)	10.55
$q_t = q_e + \frac{D_1}{m_a}\exp(-k_1 t) - \frac{D_2}{m_a}\exp(-k_2 t)$	k_2(1/min)	0.083
	R^2	0.999
	RMSE	0.018

k_{id} and k_{fd}: rate constants of the interparticle diffusion model and film diffusion, D_1 and D_2: adsorption speed parameters of the quick and slow steps (m mol/L).

thermodynamic parameters (Fig. 12), and also the Van Hoff's equations were used to determine the non-spontaneous and spontaneous processes (Table 6). As you can see, the values of ΔH°, ΔS°, and ΔG° were negative, which indicates that the process is exothermal, the increase of irregularity, and also from the negative ΔG° value, it can be concluded that the adsorption process is spontaneous [79,80]. On the other hand, the negative ΔS° indicates that the changes in the structure of the adsorbent are not significant, or in other words, the adsorbent does not change structure during the adsorption process and the adsorption process is physical. Generally, the studied thermodynamic parameters indicate that the adsorption of Deltamethrin via CS/PAA/Fe_3O_4 nanocomposite hydrogel does not require energy input and is suitable for industrial use [74,81]. The thermodynamic parameters ΔH°, ΔG°, and ΔS° were acquired negatively using Eqs. (9), (10) and (11).

$$ln(k_c) = \frac{\Delta S^o}{R} - \frac{\Delta H^o}{R}\left(\frac{1}{T}\right) \quad (9)$$

$$\Delta G^o = -RTln(k_c) \quad (10)$$

$$k_c = m\frac{q_e}{C_e} \quad (11)$$

3.7. Adsorption-desorption and reusability study

In order to investigate the desorption of Deltamethrin after adsorption by CS/PAA/Fe_3O_4 nanocomposite hydrogel, different Briton-Robinson buffer pHs were used to select the appropriate desorption

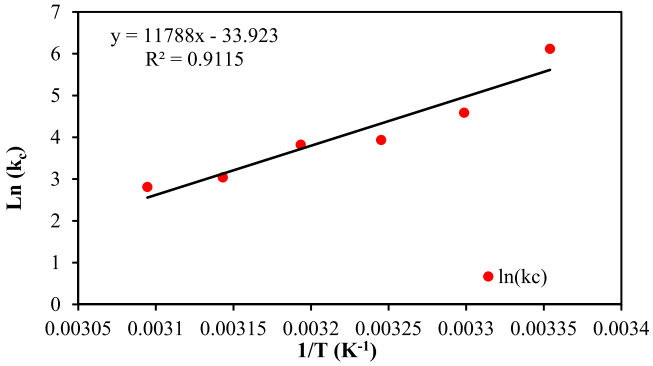

Fig. 12. Thermodynamic graph.

medium, the results are shown in Fig. 13-a. As can be seen, the maximum percentage of adsorption at pH is 2. Therefore, Adsorption-desorption were performed in a Briton-Robinson buffer medium at a pH of 2 up to 10 Cycles. The desorption results obtained from CS/PAA/Fe_3O_4 nanocomposite hydrogel show that with increasing the adsorption-desorption process steps, the adsorption capacity of the studied hydrogel is reduced; There are disparate factors such as injury to the adsorbent areas and filling the adsorbent sites with Deltamethrin [82]. In addition CS/PAA/Fe_3O_4 nanocomposite hydrogel up to ten cycles of the adsorption-desorption process as shown in (Fig. 13-b), the above adsorber can adsorb >96 %, which indicates the synthesized composite has a good ability to adsorb and desorbate Deltamethrin. This indicates that CS/PAA/Fe_3O_4 nanocomposite hydrogel can be used for both practical and industrial intention. The anion and cations effect on Deltamethrin removal was investigated and results was shown in Fig. 13-c. As can be seen, the removal percentage was decreased slightly in the presence of anions and cations, which is due to their competition with Deltamethrin to be placed on the adsorbent surface.

3.8. Results of artificial neural network

The neural network study was performed to compare and validate the (CCD-RSM) model. In an artificial neural network (ANN), experimental data is subdivided into training, validation, and experimental data, and finally, the general state in which all data is reviewed. The value of R^2 in all four data is higher than 0.92, also in the fourth part of the general data, the value of R^2 was 0.993, which shows that the artificial network has a high ability to process experimental data (Fig. 14-b). On the other hand showed the analysis of experimental data, for data modeling, the hidden layer of the 14th layer was chosen due to the low value of RMSE, which has the best performance for data modeling (Fig. 14-a). In order to assess the capabilities of the CCD model, the artificial neural network and the CCD method were compared, in this order; the evaluated data were compared with the data obtained from both models CCD, and ANN (Table 7). In the next step, the error values were examined and the error values show the difference between the accuracy of the data of the two CCD and ANN models with the real data (Table 8). Both models have low error values, indicating the high ability

Table 6
Thermodynamic parameters related to Deltamethrin adsorption by CS/PAA/Fe_3O_4 nanocomposite hydroge.

T(°C)	ΔG°(KJ/mol)	ΔH°(KJ/mol)	ΔS°(J/mol.K)
25	−15.163	−98.005	−282.04
30	−11.56		
35	−10.078		
40	−9.95		
45	−8.036		
50	−7.552		

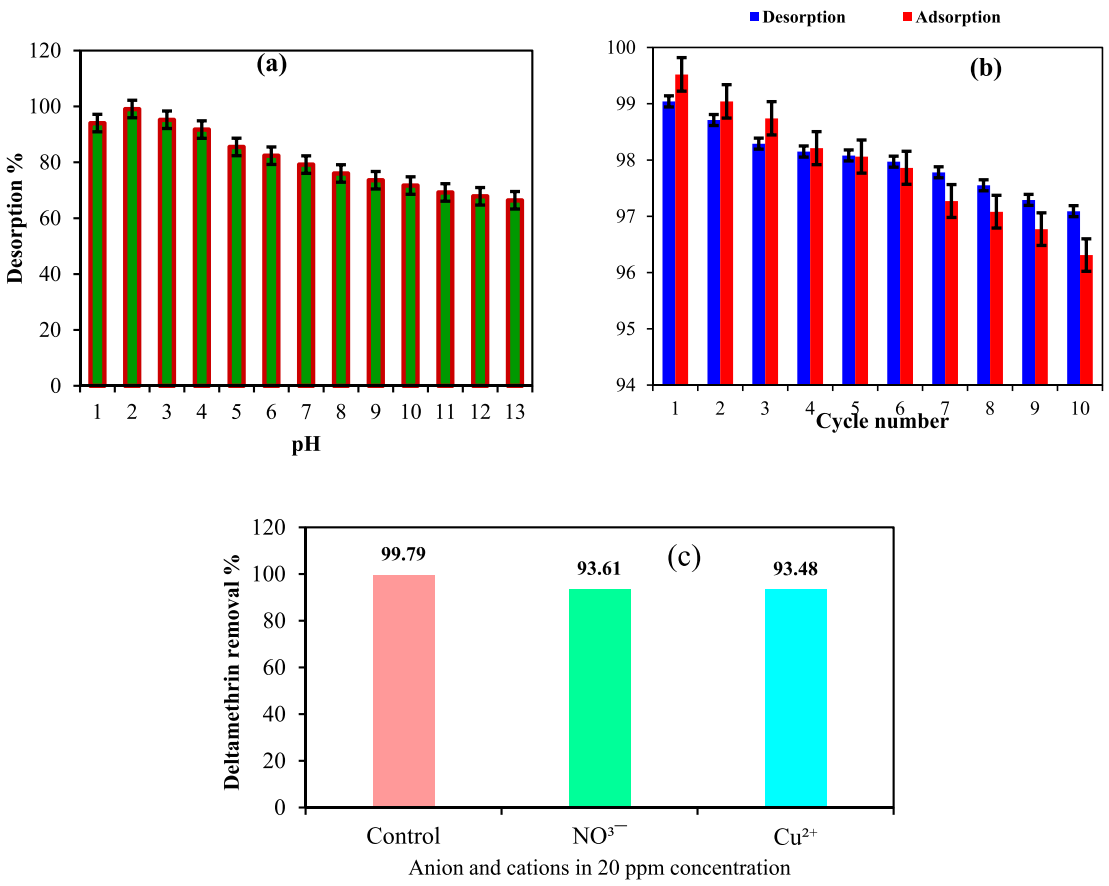

Fig. 13. a) Desorption diagram at different pHs, b) Adsorption and desorption charts, c) Anion and cations effects.

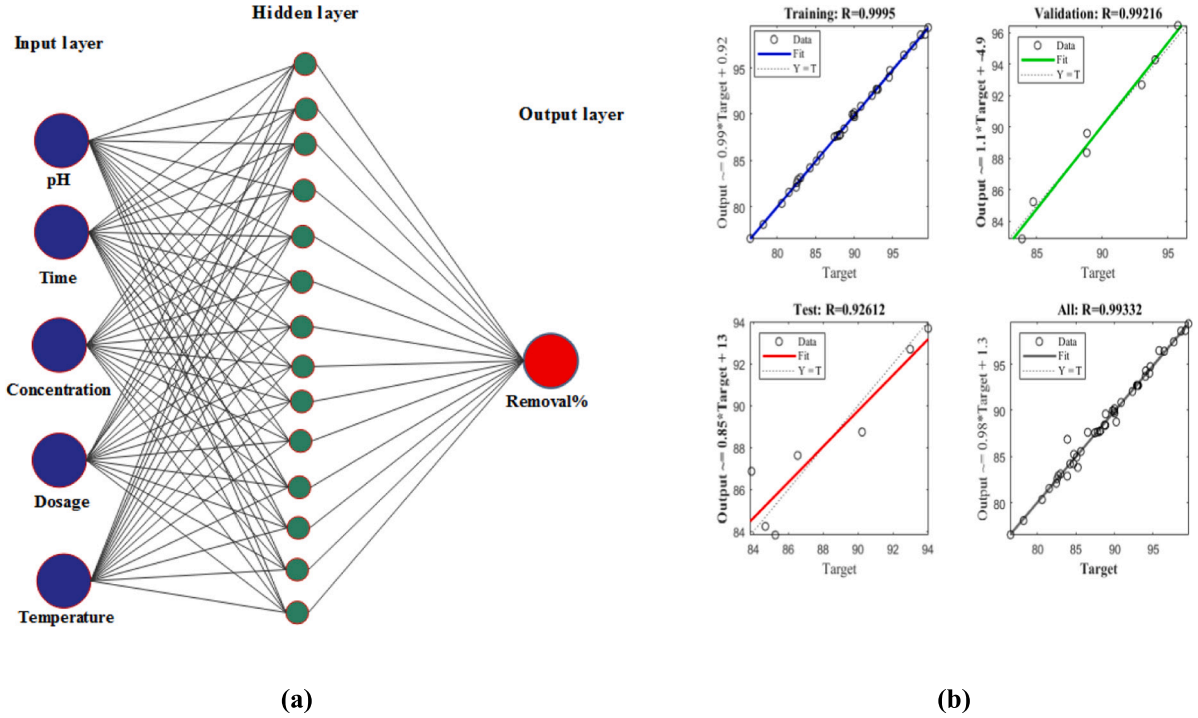

Fig. 14. The structural shape of the artificial neural network (ANN) and b) the regression diagrams for ANN.

Table 7
Comparison of real data of two central composite composites (CCD) and ANN.

No.	Actual	ANN	CCD	No.	Actual	ANN	CCD
1	87.45	87.56	87.56	24	82.45	82.09	82.45
2	89.95	89.89	90.03	25	88.83	88.37	88.94
3	90.23	88.74	90.30	26	90.86	90.84	90.88
4	92.93	92.69	93.02	27	92.32	92.03	92.41
5	83.01	83.12	82.97	28	94.52	94	94.6
6	83.89	86.86	83.91	29	83.88	82.88	83.85
7	86.53	87.62	86.61	30	84.25	84.2	84.26
8	87.79	87.66	87.79	31	88.21	87.82	88.21
9	94.64	94.73	94.68	32	88.85	89.6	88.87
10	95.78	96.46	95.92	33	82.56	82.59	82.36
11	97.68	97.39	97.77	34	85.64	85.55	85.48
12	99.19	98.63	99.26	35	82.71	82.92	82.51
13	90.01	90.16	90.07	36	90.03	89.71	89.86
14	89.76	89.96	89.77	37	99.59	99.36	99.13
15	94.04	94.27	94.05	38	88.71	88.42	88.81
16	94.01	93.68	93.99	39	85.09	84.94	84.91
17	81.52	81.54	81.61	40	98.62	98.57	98.44
18	84.74	85.25	84.79	41	96.45	96.39	96.21
19	84.68	84.23	84.73	42	85.25	83.82	85.13
20	88.07	87.7	88.16	43	93.1	92.69	93.08
21	76.51	76.55	76.55	44	92.98	92.69	93.08
22	78.19	78.07	78.2	45	92.88	92.69	93.08
23	80.59	80.35	80.56	46	93.02	92.69	93.08

Table 8
The structural shape of the artificial neural network (ANN) and b) the regression diagrams for ANN.

Performance	ANN	CCD
MAE	0.4	0.087
MAPE	0.005	0.00096
RMSE	0.647	0.121
Minimum Adsolute Error	0.02	0.1×10^{-3}
Maximum Adsolute Error	2.97	0.4595
R^2	0.987	0.999

MAPE: mean absolute percentage error, MAE: mean absolute error.

Table 9
Comparing the adsorption capacity of CS/PAA/Fe_3O_4 with the adsorption capacity of different adsorbents for Deltamethrin.

Adsorbent	Adsorbate	q_m (mg/g)	Ref.
Activated Carbon from Pistachio nutshells	Deltamethrin	162.6	[84]
Activated Carbon from Novel African walnut shell (AWS)	Deltamethrin	57.64	[85]
La-MOF	Deltamethrin	227.34	[86]
Activated Carbon	Deltamethrin	74	[87]
Clay/GO/Fe_3O_4	Diazinon	7.38	[83]
CS/PAA/Fe_3O_4	Deltamethrin	369.9	This study

of both models to express Deltamethrin adsorption experimental data. Finally, the RSM-CCD method has a higher capability in expressing data than the artificial neural network method due to lower error values [83].

3.9. Comparison with previous studies

The results (q_m) of this study were compared with others and reported in Table 9. As can be seen, the maximum capacity of CS/PAA/Fe_3O_4 is higher than other adsorbents. Also, the maximum capacity of the adsorbents that was used for Deltamethrin removal is low. Therefore, in this study CS/PAA/Fe_3O_4 was synthesized and used for Deltamethrin adsorption. Maximum capacity of CS/PAA/Fe_3O_4 is equal to 369.9 mg/g that was better and comparable to the previously reported.

4. Conclusion

In this study, the ability and adsorption capacity of CS/PAA/Fe_3O_4 nanocomposite hydrogel in the adsorption of Deltamethrin from aqueous solutions was investigated. The results of FT-IR, XRD, VSM, TGA, EDX, Map, and FE-SEM analysis showed that the CS/PAA/Fe_3O_4 nanocomposite hydrogel was properly synthesized and had a semi-crystalline structure. Also, the effect of temperature, pH, contact time, the amount of composite, and pesticide concentration on the adsorption efficiency was studied using artificial neural networks and response surface methodology. The results of this study showed that the optimum conditions for the removal of Deltamethrin using CS/PAA/Fe_3O_4 nanocomposite hydrogel are: temperature=26.07 °C, initial concentration = 22.24 mg/L, contact time = 89.72 min, nanocomposite hydrogel dosage = 1.28 g/L and the pH at 7.23, in which the adsorption efficiency is equal to 99.79 %. The results showed that the model is obtained from the response surface method had a higher predictability than the artificial neural network model. The results of the isothermal study showed that the adsorption process of Deltamethrin by this adsorbent from the three-parameter Toth isotherm model with high R^2 and low error had a better ability to express the adsorption process equilibrium; the process was reversible and physically desirable. The results of the kinetic study showed that the process of Deltamethrin adsorption by CS/PAA/Fe_3O_4 nanocomposite hydrogel follows pseudo-second-order model. In addition, the results of the adsorption mechanism study showed that the adsorption process of Deltamethrin by this adsorbent followed the Double-exponential model which is a combination of intra and inter particle diffusion. The results generally showed that the adsorption process of Deltamethrin using CS/PAA/Fe_3O_4 nanocomposite hydrogel occur both monolayer and multilayer. The results of the thermodynamic study showed that the process of adsorption of Deltamethrin by CS/PAA/Fe_3O_4 nanocomposite hydrogel is an exothermic and spontaneous process. The results of the adsorption and adsorption study showed CS/PAA/Fe_3O_4 nanocomposite hydrogel had the ability to adsorb and release the Deltamethrin pesticide for up to 10 cycles. In general, the results of this study showed that the response surface method can be used to evaluate the optimal conditions in the process of adsorption of Deltamethrin by the adsorbent. The main limitation for the practical use of the results of this study is the highly variable concentrations of the mentioned pesticide at different times. However, in this study, an appropriate concentration range was tried to be checked, but continuous monitoring of the environmental can be a suitable solution to overcome this problem.

Declaration of competing interest

The authors declare that they have no known competing financial interests or personal relationships that could have appeared to influence the work reported in this paper.

Acknowledgment

Authors gratefully acknowledge the University of Tabriz in Iran for their financial support of this work.

Data availability

Data will be made available on request.

References

[1] N.A. Tarazona, R. Machatschek, J. Balcucho, J.L. Castro-Mayorga, J.F. Saldarriaga, A. Lendlein, Opportunities and challenges for integrating the development of sustainable polymer materials within an international circular (bio) economy concept, MRS Energ. Sustain. 9 (1) (2022) 28–34.
[2] V. Sivasankarapillai, S. Das, F. Sabir, M. Sundaramahalingam, J. Colmenares, S. Prasannakumar, M. Rajan, A. Rahdar, G. Kyzas, Progress in natural polymer

engineered biomaterials for transdermal drug delivery systems, Mater. Today Chem. 19 (2021) 100382.
[3] A. Azari, M. Abtahi, S. Dobaradaran, R. Saeedi, A.R. Yari, M.H. Vaziri, S. A. Razavinasab, M. Malakoutian, K. Yaghmaeain, N. Jaafarzadeh, Polycyclic aromatic hydrocarbons in high-consumption soft drinks and non-alcoholic beers in Iran: monitoring, Monte Carlo simulations and human health risk assessment, Microchem. J. 191 (2023) 108791.
[4] X. Lin, C.T. Tsao, M. Kyomoto, M. Zhang, Injectable natural polymer hydrogels for treatment of knee osteoarthritis, Adv. Healthc. Mater. 11 (9) (2022) 2101479.
[5] S.-C. Hong, S.-Y. Yoo, H. Kim, J. Lee, Chitosan-based multifunctional platforms for local delivery of therapeutics, Mar. Drugs 15 (3) (2017) 60.
[6] M.C. Catoira, L. Fusaro, D. Di Francesco, M. Ramella, F. Boccafoschi, Overview of natural hydrogels for regenerative medicine applications, J. Mater. Sci. Mater. Med. 30 (10) (2019) 1–10.
[7] J.-S. Ahn, H.-K. Choi, M.-K. Chun, J.-M. Ryu, J.-H. Jung, Y.-U. Kim, C.-S. Cho, Release of triamcinolone acetonide from mucoadhesive polymer composed of chitosan and poly (acrylic acid) in vitro, Biomaterials 23 (6) (2002) 1411–1416.
[8] A.H. Karoyo, L.D. Wilson, A review on the design and hydration properties of natural polymer-based hydrogels, Materials 14 (5) (2021) 1095.
[9] L.C. Oliveira, R.V. Rios, J.D. Fabris, K. Sapag, V.K. Garg, R.M. Lago, Clay–iron oxide magnetic composites for the adsorption of contaminants in water, Appl. Clay Sci. 22 (4) (2003) 169–177.
[10] S. Sidik, S. Triwahyono, A. Jalil, Z. Majid, N. Salamun, N. Talib, T. Abdullah, CO2 reforming of CH4 over Ni–Co/MSN for syngas production: role of Co as a binder and optimization using RSM, Chem. Eng. J. 295 (2016) 1–10.
[11] R. Bazargan-Lari, H.R. Zafarani, M.E. Bahrololoom, A. Nemati, Removal of Cu (II) ions from aqueous solutions by low-cost natural hydroxyapatite/chitosan composite: equilibrium, kinetic and thermodynamic studies, J. Taiwan Inst. Chem. Eng. 45 (4) (2014) 1642–1648.
[12] A.H. Zainuddin, S.Y. Wee, A.Z. Aris, Occurrence and potential risk of organophosphorus pesticides in urbanised Linggi River, Negeri Sembilan, Malaysia, Environ. Geochem. Health 42 (11) (2020) 3703–3715.
[13] A. Kiani, M. Ahmadloo, M. Moazzen, N. Shariatifar, S. Shahsavari, M. Arabameri, M.M. Hasani, A. Azari, M.A. Abdel-Wahhab, Monitoring of polycyclic aromatic hydrocarbons and probabilistic health risk assessment in yogurt and butter in Iran, Food Sci. Nutr. 9 (4) (2021) 2114–2128.
[14] J. Nie, Y. Sun, Y. Zhou, M. Kumar, M. Usman, J. Li, J. Shao, L. Wang, D.C. Tsang, Bioremediation of water containing pesticides by microalgae: mechanisms, methods, and prospects for future research, Sci. Total Environ. 707 (2020) 136080.
[15] A. Kouhpayeh, M. Moazzen, G.R. Jahed Khaniki, S. Dobaradaran, N. Shariatifar, M. Ahmadloo, A. Azari, S. Nazmara, A. Kiani, M. Salari, Extraction and determination of phthalate esters (PAEs) in Doogh, J. Mazandaran Univ. Med. Sci. 26 (145) (2017) 257–267.
[16] R. RezaeiKalantary, A. JonidiJafari, B. Kakavandi, S. Nasseri, A. Ameri, A. Azari, Adsorption and magnetic separation of lead from synthetic wastewater using carbon/iron oxide nanoparticles composite, J. Mazandaran Univ. Med. Sci. 24 (113) (2014) 172–183.
[17] W. Tang, D. Wang, J. Wang, Z. Wu, L. Li, M. Huang, S. Xu, D. Yan, Pyrethroid pesticide residues in the global environment: an overview, Chemosphere 191 (2018) 990–1007.
[18] Q. Lu, Y. Sun, I. Ares, A. Anadón, M. Martínez, M.-R. Martínez-Larrañaga, Z. Yuan, X. Wang, M.-A. Martínez, Deltamethrin toxicity: a review of oxidative stress and metabolism, Environ. Res. 170 (2019) 260–281.
[19] H. Pasalari, H.R. Ghaffari, A.H. Mahvi, M. Pourshabanian, A. Azari, Activated carbon derived from date stone as natural adsorbent for phenol removal from aqueous solution, Desalin. Water Treat. 72 (2017) 406–417.
[20] F.d.S. Cunha, N.d.C. Sousa, R.F.B. Santos, J.O. Meneses, M.V.S. do Couto, F.T.C. de Almeida, J.G. de Sena Filho, P.C.F. Carneiro, A.N. Maria, R.Y. Fujimoto, Deltamethrin-induced nuclear erythrocyte alteration and damage to the gills and liver of Colossoma macropomum, Environ. Sci. Pollut. Res. 25 (15) (2018) 15102–15110.
[21] S. Cosgrove, B. Jefferson, P. Jarvis, Pesticide removal from drinking water sources by adsorption: a review, Environ. Technol. Rev. 8 (1) (2019) 1–24.
[22] M. Radwan, J. Jurewicz, B. Wielgomas, M. Piskunowicz, W. Sobala, P. Radwan, L. Jakubowski, W. Hawuła, W. Hanke, The association between environmental exposure to pyrethroids and sperm aneuploidy, Chemosphere 128 (2015) 42–48.
[23] M. Koureas, A. Tsakalof, A. Tsatsakis, C. Hadjichristodoulou, Systematic review of biomonitoring studies to determine the association between exposure to organophosphorus and pyrethroid insecticides and human health outcomes, Toxicol. Lett. 210 (2) (2012) 155–168.
[24] R. Ding, Z. Cao, Y. Wang, X. Gao, H. Luo, C. Zhang, S. Ma, X. Ma, H. Jin, C. Lu, The implication of p66shc in oxidative stress induced by deltamethrin, Chem. Biol. Interact. 278 (2017) 162–169.
[25] L. Xie, L. Zhou, L. Li, X. Xie, Y. Li, Preparation and adsorption selectivity of deltamethrin molecularly imprinted polymers by two-step seed swelling method, J. Appl. Polym. Sci. 136 (16) (2019) 47415.
[26] I.A. Saleh, N. Zouari, M.A. Al-Ghouti, Removal of pesticides from water and wastewater: chemical, physical and biological treatment approaches, Environ. Technol. Innov. 19 (2020) 101026.
[27] T.S. de Almeida Lopes, R. Hessler, C. Bohner, G.B.A. Junior, R.F. de Sena, Pesticides removal from industrial wastewater by a membrane bioreactor and post-treatment with either activated carbon, reverse osmosis or ozonation, J. Environ. Chem. Eng. 8 (6) (2020) 104538.
[28] O.G. Júnior, M.G.B. Santos, A.B. Nossol, M.C.V. Starling, A.G. Trovó, Decontamination and toxicity removal of an industrial effluent containing pesticides via multistage treatment: coagulation-flocculation-settling and photo-Fenton process, Process. Saf. Environ. Prot. 147 (2021) 674–683.
[29] A. Lajevardi, M.T. Yaraki, A. Masjedi, A. Nouri, M.H. Sadr, Green synthesis of MOF@ Ag nanocomposites for catalytic reduction of methylene blue, J. Mol. Liq. 276 (2019) 371–378.
[30] D. Vaya, P.K. Surolia, Semiconductor based photocatalytic degradation of pesticides: an overview, Environ. Technol. Innov. 20 (2020) 101128.
[31] S.Y. Hashemi, M. Yegane Badi, H. Pasalari, A. Azari, H. Arfaeinia, A. Kiani, Degradation of ceftriaxone from aquatic solution using a heterogeneous and reusable O3/UV/Fe3O4@ TiO2 systems: operational factors, kinetics and mineralisation, Int. J. Environ. Anal. Chem. 102 (18) (2022) 6904–6920.
[32] H. Li, F. Wang, J. Li, S. Deng, S. Zhang, Adsorption of three pesticides on polyethylene microplastics in aqueous solutions: kinetics, isotherms, thermodynamics, and molecular dynamics simulation, Chemosphere 264 (2021) 128556.
[33] S.A. Mousavi, B. Kamarehie, A. Almasi, M. Darvishmotevalli, M. Salari, M. Moradnia, F. Azimi, M. Ghaderpoori, Z. Neyazi, M.A. Karami, Removal of Rhodamine B from aqueous solution by stalk corn activated carbon: adsorption and kinetic study, Biomass Convers. Biorefinery 13 (9) (2023) 7927–7936.
[34] M.A. Zazouli, A. Azari, S. Dehghan, R. Salmani Malekkolae, Adsorption of methylene blue from aqueous solution onto activated carbons developed from eucalyptus bark and Crataegus oxyacantha core, Water Sci. Technol. 74 (9) (2016) 2021–2035.
[35] A. Mojiri, J.L. Zhou, B. Robinson, A. Ohashi, N. Ozaki, T. Kindaichi, H. Farraji, M. Vakili, Pesticides in aquatic environments and their removal by adsorption methods, Chemosphere 253 (2020) 126646.
[36] M.Y. Badi, A. Azari, A. Esrafili, E. Ahmadi, M. Gholami, Performance evaluation of magnetized multiwall carbon nanotubes by iron oxide nanoparticles in removing fluoride from aqueous solution, J. Mazandaran Univ. Med. Sci. 25 (124) (2015) 128–142.
[37] A. Esrafili, R. Rezaei Kalantary, A. Azari, E. Ahmadi, M. Gholami, Removal of diethyl phthalate from aqueous solution using persulfate-based (UV/Na2S2O8/Fe2+) advanced oxidation process, J. Mazandaran Univ. Med. Sci. 25 (132) (2016) 122–135.
[38] E. Alver, A.Ü. Metin, F. Brouers, Methylene blue adsorption on magnetic alginate/rice husk bio-composite, Int. J. Biol. Macromol. 154 (2020) 104–113.
[39] M. Vakili, S. Deng, G. Cagnetta, W. Wang, P. Meng, D. Liu, G. Yu, Regeneration of chitosan-based adsorbents used in heavy metal adsorption: a review, Sep. Purif. Technol. 224 (2019) 373–387.
[40] M. Tanzifi, M.T. Yaraki, Z. Beiramzadeh, L.H. Saremi, M. Najafifard, H. Moradi, M. Mansouri, M. Karami, H. Bazgir, Carboxymethyl cellulose improved adsorption capacity of polypyrrole/CMC composite nanoparticles for removal of reactive dyes: experimental optimization and DFT calculation, Chemosphere 255 (2020) 127052.
[41] A.R. Bagheri, M. Ghaedi, A. Asfaram, A.A. Bazrafshan, R. Jannesar, Comparative study on ultrasonic assisted adsorption of dyes from single system onto Fe3O4 magnetite nanoparticles loaded on activated carbon: experimental design methodology, Ultrason. Sonochem. 34 (2017) 294–304.
[42] Y. Tian, H. Ma, B. Xing, Preparation of surfactant modified magnetic expanded graphite composites and its adsorption properties for ionic dyes, Appl. Surf. Sci. 537 (2021) 147995.
[43] E. Tahmasebi, Y. Yamini, Facile synthesis of new nano sorbent for magnetic solid-phase extraction by self assembling of bis-(2, 4, 4-trimethyl pentyl)-dithiophosphinic acid on Fe3O4@ Ag core@ shell nanoparticles: characterization and application, Anal. Chim. Acta 756 (2012) 13–22.
[44] K. Kheiri, N. Sohrabi, R. Mohammadi, M.S. Amini-Fazl, Preparation and characterization of magnetic nanohydrogel based on chitosan for 5-fluorouracil drug delivery and kinetic study, Int. J. Biol. Macromol. 202 (2022) 191–198.
[45] A. Azari, R. Nabizadeh, A.H. Mahvi, S. Nasseri, Magnetic multi-walled carbon nanotubes-loaded alginate for treatment of industrial dye manufacturing effluent: adsorption modelling and process optimisation by central composite face-central design, Int. J. Environ. Anal. Chem. 103 (7) (2023) 1509–1529.
[46] A. Tadjarodi, S.M. Ferdowsi, R. Zare-Dorabei, A. Barzin, Highly efficient ultrasonic-assisted removal of Hg (II) ions on graphene oxide modified with 2-pyridinecarboxaldehyde thiosemicarbazone: adsorption isotherms and kinetics studies, Ultrason. Sonochem. 33 (2016) 118–128.
[47] N. Shahbazi, R. Zare-Dorabei, Probe for sensitive direct determination of sulphide ions based on gold nanoparticles, IET Nanobiotechnol. 12 (8) (2018) 1140–1143.
[48] B.R. Broujeni, A. Nilchi, F. Azadi, Adsorption modeling and optimization of thorium (IV) ion from aqueous solution using chitosan/TiO2 nanocomposite: application of artificial neural network and genetic algorithm, Environ. Nanotechnol. Monit. Manag. 15 (2021) 100400.
[49] H. Mashhadimoslem, M. Vafaeinia, M. Safarzadeh, A. Ghaemi, F. Fathalian, A. Maleki, Development of predictive models for activated carbon synthesis from different biomass for CO2 adsorption using artificial neural networks, Ind. Eng. Chem. Res. 60 (38) (2021) 13950–13966.
[50] A. Azari, R. Nabizadeh, A.H. Mahvi, S. Nasseri, Integrated Fuzzy AHP-TOPSIS for selecting the best color removal process using carbon-based adsorbent materials: multi-criteria decision making vs. systematic review approaches and modeling of textile wastewater treatment in real conditions, Int. J. Environ. Anal. Chem. 102 (18) (2022) 7329–7344.
[51] H. Karimi, M. Ghaedi, Application of artificial neural network and genetic algorithm to modeling and optimization of removal of methylene blue using activated carbon, J. Ind. Eng. Chem. 20 (4) (2014) 2471–2476.
[52] S. Zhang, Y. Zhou, W. Nie, L. Song, Preparation of Fe3O4/chitosan/poly (acrylic acid) composite particles and its application in adsorbing copper ion (II), Cellulose 19 (6) (2012) 2081–2091.

[53] M. Pooresmaeil, Y. Mansoori, M. Mirzaeinejad, A. Khodayari, Efficient removal of methylene blue by novel magnetic hydrogel nanocomposites of poly (acrylic acid), Adv. Polym. Technol. 37 (1) (2018) 262–274.
[54] X.-Y. Sun, R.-T. Ma, J. Chen, Y.-P. Shi, Magnetic boronate modified molecularly imprinted polymers on magnetite microspheres modified with porous TiO2 (Fe3O4@ pTiO2@ MIP) with enhanced adsorption capacity for glycoproteins and with wide operational pH range, Microchim. Acta 185 (12) (2018) 1–10.
[55] J.P. Fan, D.D. Liao, Y.L. Xie, B. Zheng, J.X. Yu, Y.H. Cao, X.H. Zhang, H.L. Peng, A molecular imprinted polymer on the surface of superparamagnetic Fe3O4–graphene oxide (MIP@ Fe3O4@ GO) for simultaneous recognition and enrichment of evodiamine and rutaecarpine in Evodiae fructus, J. Appl. Polym. Sci. 134 (7) (2017).
[56] J. Zhang, Q. Wang, A. Wang, Synthesis and characterization of chitosan-g-poly (acrylic acid)/attapulgite superabsorbent composites, Carbohydr. Polym. 68 (2) (2007) 367–374.
[57] Y. Chen, H.-m. Tan, Crosslinked carboxymethylchitosan-g-poly (acrylic acid) copolymer as a novel superabsorbent polymer, Carbohydr. Res. 341 (7) (2006) 887–896.
[58] S. Moulay, N. Bensacia, Removal of heavy metals by homolytically functionalized poly (acrylic acid) with hydroquinone, Int. J. Ind. Chem. 7 (4) (2016) 369–389.
[59] S.C. Dey, M. Al-Amin, T.U. Rashid, M.Z. Sultan, M. Ashaduzzaman, M. Sarker, S. M. Shamsuddin, Preparation, characterization and performance evaluation of chitosan as an adsorbent for remazol red, Int. J. Latest Res. Eng. Technol. 2 (2) (2016) 52–62.
[60] A. Asfaram, M. Ghaedi, G.R. Ghezelbash, E.A. Dil, I. Tyagi, S. Agarwal, V.K. Gupta, Biosorption of malachite green by novel biosorbent Yarrowia lipolytica isf7: application of response surface methodology, J. Mol. Liq. 214 (2016) 249–258.
[61] M. Tazik, M.H. Dehghani, K. Yaghmaeian, S. Nazmara, M. Salari, A.H. Mahvi, S. Nasseri, H. Soleimani, R.R. Karri, 4-Chlorophenol adsorption from water solutions by activated carbon functionalized with amine groups: response surface method and artificial neural networks, Sci. Rep. 13 (1) (2023) 7831.
[62] X. Shi, A. Karachi, M. Hosseini, M.S. Yazd, H. Kamyab, M. Ebrahimi, Z. Parsaee, Ultrasound wave assisted removal of Ceftriaxone sodium in aqueous media with novel nano composite g-C3N4/MWCNT/Bi2WO6 based on CCD-RSM model, Ultrason. Sonochem. 68 (2020) 104460.
[63] A.R. Bagheri, M. Ghaedi, A. Asfaram, R. Jannesar, A. Goudarzi, Design and construction of nanoscale material for ultrasonic assisted adsorption of dyes: application of derivative spectrophotometry and experimental design methodology, Ultrason. Sonochem. 35 (2017) 112–123.
[64] J.-T. Horng, N.-M. Liu, K.-T. Chiang, Investigating the machinability evaluation of Hadfield steel in the hard turning with Al2O3/TiC mixed ceramic tool based on the response surface methodology, J. Mater. Process. Technol. 208 (1–3) (2008) 532–541.
[65] S. Saini, J. Chawla, R. Kumar, I. Kaur, Response surface methodology (RSM) for optimization of cadmium ions adsorption using C16-6-16 incorporated mesoporous MCM-41, SN Appl. Sci. 1 (8) (2019) 1–10.
[66] D.C. Montgomery, Design and Analysis of Experiments, John wiley & sons, 2017.
[67] R. Foroutan, R. Mohammadi, S. Farjadfard, H. Esmaeili, B. Ramavandi, G.A. Sorial, Eggshell nano-particle potential for methyl violet and mercury ion removal: surface study and field application, Adv. Powder Technol. 30 (10) (2019) 2188–2199.
[68] S.M. Taha, M.E. Amer, A.E. Elmarsafy, M.Y. Elkady, Adsorption of 15 different pesticides on untreated and phosphoric acid treated biochar and charcoal from water, J. Environ. Chem. Eng. 2 (4) (2014) 2013–2025.
[69] D. Jiang, Y. Yang, C. Huang, M. Huang, J. Chen, T. Rao, X. Ran, Removal of the heavy metal ion nickel (II) via an adsorption method using flower globular magnesium hydroxide, J. Hazard. Mater. 373 (2019) 131–140.
[70] M.H. Dehghani, S. Kamalian, M. Shayeghi, M. Yousefi, Z. Heidarinejad, S. Agarwal, V.K. Gupta, High-performance removal of diazinon pesticide from water using multi-walled carbon nanotubes, Microchem. J. 145 (2019) 486–491.
[71] G. Moussavi, H. Hosseini, A. Alahabadi, The investigation of diazinon pesticide removal from contaminated water by adsorption onto NH4Cl-induced activated carbon, Chem. Eng. J. 214 (2013) 172–179.
[72] D. Bingol, N. Tekin, M. Alkan, Brilliant Yellow dye adsorption onto sepiolite using a full factorial design, Appl. Clay Sci. 50 (3) (2010) 315–321.
[73] L. Guo, G. Liu, R.-Y. Hong, H.-Z. Li, Preparation and characterization of chitosan poly (acrylic acid) magnetic microspheres, Mar. Drugs 8 (7) (2010) 2212–2222.
[74] S. Ladnorg, N.L. Junior, P. Dall, D.G. Domingos, B.S. Magnus, M. Wichern, T. Gehring, R.H.R. da Costa, Alginate-like exopolysaccharide extracted from aerobic granular sludge as biosorbent for methylene blue: thermodynamic, kinetic and isotherm studies, J. Environ. Chem. Eng. 7 (3) (2019) 103081.
[75] M.T. Yagub, T.K. Sen, H. Ang, Equilibrium, kinetics, and thermodynamics of methylene blue adsorption by pine tree leaves, Water Air Soil Pollut. 223 (8) (2012) 5267–5282.
[76] A. Deb, M. Kanmani, A. Debnath, K.L. Bhowmik, B. Saha, Ultrasonic assisted enhanced adsorption of methyl orange dye onto polyaniline impregnated zinc oxide nanoparticles: kinetic, isotherm and optimization of process parameters, Ultrason. Sonochem. 54 (2019) 290–301.
[77] P. Wadhera, R. Jindal, R. Dogra, Synthesis of semi interpenetrating network hydrogel [(GrA-Psy)-cl-Poly (AA)] and its application for efficient removal of malachite green from aqueous solution, Polym. Eng. Sci. 59 (7) (2019) 1416–1427.
[78] N. Mohammadi, H. Khani, V.K. Gupta, E. Amereh, S. Agarwal, Adsorption process of methyl orange dye onto mesoporous carbon material–kinetic and thermodynamic studies, J. Colloid Interface Sci. 362 (2) (2011) 457–462.
[79] Q. Kong, Y.-n. Wang, L. Shu, M.-s. Miao, Isotherm, kinetic, and thermodynamic equations for cefalexin removal from liquids using activated carbon synthesized from loofah sponge, Desalin. Water Treat. 57 (17) (2016) 7933–7942.
[80] A. Alahabadi, N. Shomoossi, F. Riahimanesh, M. Salari, Development of AC/ZnO/Fe2O3 for efficiently adsorptive removal of Tetracycline from water environment: isotherm, kinetic and thermodynamic studies and adsorption mechanism, Biomass Convers. Biorefinery (2023) 1–19.
[81] G. Asgari, A. Seid-mohammadi, A. Rahmani, M.T. Samadi, S. Alizadeh, D. Nematollahi, M. Salari, Carbon felt modified with N-doped rGO for an efficient electro-peroxone process in diuron degradation and biodegradability improvement of wastewater from a pesticide manufacture: optimization of process parameters, electrical energy consumption and degradation pathway, Sep. Purif. Technol. 274 (2021) 118962.
[82] W. Huang, Z.-m. Liu, Biosorption of Cd (II)/Pb (II) from aqueous solution by biosurfactant-producing bacteria: isotherm kinetic characteristic and mechanism studies, Colloids Surf. B: Biointerfaces 105 (2013) 113–119.
[83] N. Sohrabi, R. Mohammadi, H.R. Ghassemzadeh, S.S.S. Heris, Equilibrium, kinetic and thermodynamic study of diazinon adsorption from water by clay/GO/Fe3O4: modeling and optimization based on response surface methodology and artificial neural network, J. Mol. Liq. 328 (2021) 115384.
[84] A. Hassan, A. Youssef, P. Priecel, Removal of deltamethrin insecticide over highly porous activated carbon prepared from pistachio nutshells, Carbon Lett. 14 (4) (2013) 234–242.
[85] O.A. Oba, N. Pasaoglulari Aydinlik, Preparation of mesoporous activated carbon from novel African walnut shells (AWS) for deltamethrin removal: kinetics and equilibrium studies, Appl Water Sci 12 (7) (2022) 149.
[86] F. Alkhatib, S.F. Ibarhiam, A.F. Alrefaei, S.H. Alrefaee, R. Pashameah, T. M. Habeebullah, S.D. Al-Qahtani, N.M. El-Metwaly, Efficient removal of deltamethrin from aqueous solutions using a novel lanthanum metal–organic framework: adsorption models and optimization via Box–Behnken design, ACS Omega 8 (35) (2023) 32130–32145.
[87] M.N. Ettish, G.S. El-Sayyad, D. Wong, M.A. Elsayed, O. Abuzalat, Efficient removal of Deltamethrin (pyrethroid ester insecticide) from water using novel chemically activated carbon derived from the inner stem bark of *C. Verum* tree, Appl. Surf. Sci. Adv. 9 (2022) 100245.